JGR Earth Surface

RESEARCH ARTICLE
10.1029/2024JF008116

A Mass Conservation Model to Study the Evolution of Coastal Soft Cliffs Driven by Sea Level Rise Over Multi-Century Timescales

M. Appleton[1,2], **R. Briganti**[1], **N. Dodd**[1], **and A. Payo**[2]

[1]Faculty of Engineering, University of Nottingham, Nottingham, UK, [2]British Geological Survey, Nottingham, UK

Key Points:

- A mathematical model suited for predicting multi-century soft cliff coastal evolution in response to sea level rise is presented
- Long-term behaviors including equilibrium and changes in coastal typology are derived analytically
- An example application shows the importance of topography for predicting coastal evolution and estimates a timescale of typology change

Correspondence to:

M. Appleton,
mapp1@bgs.ac.uk;
matthew.appleton1@nottingham.ac.uk

Citation:

Appleton, M., Briganti, R., Dodd, N., & Payo, A. (2026). A mass conservation Model to study the evolution of coastal soft cliffs driven by sea level rise over multi-century timescales. *Journal of Geophysical Research: Earth Surface*, *131*, e2024JF008116. https://doi.org/10.1029/2024JF008116

Received 24 OCT 2024
Accepted 5 JAN 2026

Author Contributions:

Conceptualization: M. Appleton, R. Briganti, A. Payo
Formal analysis: M. Appleton, A. Payo
Funding acquisition: R. Briganti, N. Dodd, A. Payo
Investigation: M. Appleton, R. Briganti, N. Dodd
Methodology: M. Appleton, R. Briganti, N. Dodd, A. Payo
Project administration: R. Briganti
Resources: R. Briganti
Software: M. Appleton
Supervision: R. Briganti, N. Dodd, A. Payo
Visualization: M. Appleton
Writing – original draft: M. Appleton
Writing – review & editing: M. Appleton, R. Briganti, N. Dodd, A. Payo

Abstract Soft cliffed coasts are particularly vulnerable to erosion and their retreat depends on environmental, geological and geomechanical factors. In this work, we use a mathematical modeling approach to understand effects of future global sea level rise on these coasts over multiple centuries. We develop a simple mass conservation model, equating material eroded from a cliff to the sediment required for foreshore adaptation to sea level rise. The model considers geological differences between cliff and beach sediment, variable and uncertain rates of sea level rise, and the complex inland topography a cliff may erode through. The model is solved analytically, and long-term behaviors discussed, including conditions for an equilibrium recession rate or a change in coastal typology. Methods for obtaining estimates of model parameters are detailed and an application of the depth of closure concept to multi-century timescales proposed. The model is applied to the Holderness coast, United Kingdom. It predicts an acceleration of cliff retreat due to rising sea levels over the next centuries, though local topographical features may cause temporary deceleration. No long-term equilibrium behavior is identified. The study also estimates that vulnerable locations along this coast will experience a change in coastal typology within the next few hundred years. These findings highlight the importance of inland topography in determining an eroding cliffed coast's resilience to sea level rise. We propose that the relative sea level rise corresponding to typology change should be used as an indicator of cliff resilience to sea level rise, instead of current cliff height.

Plain Language Summary Soft cliff erosion threatens natural and anthropized environments. Accelerating sea level rise caused by climate change is expected to accelerate erosion, however the future evolution of these coasts is uncertain. We have developed a simple model suitable for exploring how erosion rates may change under global sea level rise scenarios. Our model allows a variable, uncertain rate of sea level rise and accounts for realistic inland topographies. From the mathematical solution to the model we estimate long-term behaviors that can happen. Either equilibrium occurs, where the cliff height stays constant as sea level rises, or the cliff height reaches zero, a scenario referred to as change in coastal typology. We apply this model to a case study: the Holderness Coast, United Kingdom, and model the effects of sea level rise scenarios on erosion rates and the time taken for the change in coastal typology to occur. We find that topography is important in determining long-term coastal change. The inland relief of the Holderness coast means that equilibrium cannot happen. Typology changes are estimated to occur at some locations on the coast over the next few hundred years. This study is important to understand unmanaged coastal evolution in a changing climate.

1. Introduction

Coastal erosion threatens communities around the world, affecting natural and anthropized environments. Soft cliffed coasts are characterized by a cliff made of erodible material, such as fractured rocks or clay, a foreshore, usually composed of sand or gravel, and an underlying shore platform. They are especially sensitive to changes in sea level (Bray & Hooke, 1997) and erode quickly due to their geomechanical properties (Hobbs et al., 2008, 2013; Lee, 2002).

Climate change induced by the emission of greenhouse gases is expected to accelerate global sea level rise (GSLR) (Glavovic et al., 2022; Oppenheimer et al., 2020). However, exploratory modeling predicts global sea level to rise by 25–50 m over the next 10,000 years, depending on carbon emissions scenarios (Clark et al., 2016; Van Breedam et al., 2020). Soft cliff retreat is expected to accelerate under increased rates of GSLR (Bray & Hooke, 1997; Payo et al., 2020), but in some circumstances an equilibrium retreat rate or deceleration may be possible (Wolinsky & Murray, 2009). A higher sea level exposes cliffs to additional wave attack, and in some

areas, climate change will also alter wave climates, possibly creating larger and more frequent erosive waves (Reguero et al., 2019). If global sea level rose by 25–50 m over the aforementioned time scales, this would have a dramatic impact on coastal areas, potentially inducing a change in coastal typology: a cliffed environment forced by substantial RSLR (Relative Sea Level Rise) could transition into another type. Typology changes are an example of climate-change tipping points of a coastal system, which may have major and irreversible consequences for local settlements, infrastructure and ecosystems (Barnard et al., 2021). Coastal retreat models driven by uncertain RSLR over these multi-century timescales are useful for coastal planning, and for exploring potential effects of sea level rise on unmanaged natural cliffed coasts.

Existing models of soft cliff erosion (Limber et al., 2018; Lopez De San Roman Blanco et al., 2019; Murray et al., 2021; Payo et al., 2016; Ranasinghe, 2020; Walkden & Hall, 2005) range in complexity and applicability from simple transect-based approaches (Limber et al., 2018) to three-dimensional (3D) modeling frameworks (Payo et al., 2016). At the timescales of interest we do not model in detail the cliff collapse mechanisms (Castedo et al., 2012; Walkden & Hall, 2005), include temporary coastal defenses (Dornbusch & Mylroie, 2018; Hudson et al., 2015; Lee, 2018; Payo & Walkden, 2018), or incorporate seasonal variations in wave attack (Dean, 1991), since these processes affect coastal evolution over a shorter timescale than a multi-century modeling period (Lopez De San Roman Blanco et al., 2019). Sea level and wind waves are fundamental drivers of shoreline change (Bosboom & Stive, 2021) but the literature shows a lack of consensus in future trends in wave climate (Bricheno et al., 2023; De Leo et al., 2023; Groll et al., 2014).

Following the categories of modeling approach proposed by Wolinsky (2009), multi-century simulations require a mesoscale modeling approach, which relies on a sediment mass balance approach to predict morphological change (Bray & Hooke, 1997; Bruun, 1962; Walkden & Hall, 2005, 2011; Wolinsky & Murray, 2009). The governing equations of many mesoscale models can be derived directly from sediment conservation principles (Wolinsky, 2009; Wolinsky & Murray, 2009) under a number of assumptions (detailed below). We will refer to models in this category as mass conservation models hereinafter. Among them, the Bruun rule (Bruun, 1962) is commonly used for studying the retreat of gently sloped shorefaces. It was extended to soft cliffed coasts by Bray and Hooke (1997), and then generalized to include a time-varying cliff height (due to both RSLR and a cliff retreating through sloping backshore topography) by Wolinsky and Murray (2009). The central idea of mass conservation models is that sediment from cliff retreat fuels accommodation (Swift & Thorne, 1992), the process by which beaches respond to sea level rise. It is assumed that as the sea level rises, the beach profile shifts upwards at the same rate, due to increased wave erosion on the upper shoreface, and decreased wave erosion on the lower shoreface. This implicitly assumes that the wave climate is stationary over the modeling period (D'Anna et al., 2021).

The beach is represented by an equilibrium profile of constant cross-shore length, depth (difference in elevation between the top of the beach and the offshore boundary of the profile) and shape, stretching to the point of closure (Nicholls et al., 1998; Ortiz & Ashton, 2016). Wolinsky and Murray (2009) show that model predictions do not depend on the exact shape of the beach equilibrium profile, many of which have been proposed (Bodge, 1992; Dean, 1991; Pilkey et al., 1993). Similar assumptions on accommodation and equilibrium beach profiles have been used to derive models for the adaptation of other coastal typologies to RSLR, including dune-beach systems (Rosati et al., 2013), barrier islands (Wolinsky & Murray, 2009) and sandy coasts protected by a seawall (Beuzen et al., 2018).

One core concept of cliff retreat modeling is that of an equilibrium retreat rate (Ashton et al., 2011): if we keep the rate of RSLR constant, will cliff recession approach some constant rate? Knowledge of the occurrence of an equilibrium rate, and the timescale of equilibrium approach, would allow us to make an assessment of how much cliff retreat might accelerate or decelerate as sea level rises. In the model of Wolinsky and Murray (2009), the possibility of an equilibrium cliff recession rate depends purely on profile geometry, independent of the rate of sea level rise.

There are two assumptions which currently restrict the ability of mass conservation models to make multi-century predictions of change on soft cliffed coasts. The first is that of a constant rate of RSLR. Recent studies predict, in general, an acceleration of GSLR in the next millennia (Fox-Kemper et al., 2021), followed by a deceleration (Clark et al., 2016; Van Breedam et al., 2020), although these scenarios come with significant uncertainty. The second limitation is the assumption of a simplified backshore topography, with constant inland slope. Long-term

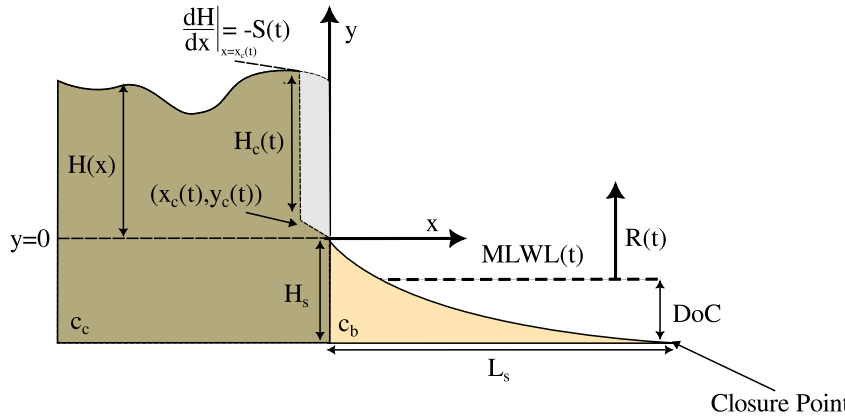

Figure 1. An eroding soft cliffed coast consisting of a cliff (darker brown region) and beach (lighter brown region) is approximated by a 2D schematic representation. The light-gray shaded region, between $x_c(0)$ and $x_c(t)$, indicates the cliff which has been eroded by time t. The origin of the x and y axes is centered at the initial position of the cliff toe. An equilibrium beach profile of constant cross-shore length L_s, depth H_s and shape stretches seawards from this point to the closure point. The depth of closure is DoC, relative to the MLWL. The inland topography $H(x)$ is relative to a fixed elevation $y = 0$. The changing tangential inland slope $S(t)$ can be calculated from $H(x)$. The cliff height $H_c(t)$ is measured relative to the moving cliff toe $(x_c(t), y_c(t))$. The sand concentrations of the cliff, c_c, and beach, c_b, are indicated, along with the rate of RSLR $R(t)$. Figure created by the lead author. © University of Nottingham.

behavior is sensitive to the value of this inland slope (Wolinsky & Murray, 2009), but finding a representative value is difficult, since it is unclear how far inland from the cliff toe this measurement should be taken.

Therefore, these two limitations must be removed so as to tailor a model toward long-term predictions, letting cliff recession be driven by realistic sea level rise scenarios, quantifying uncertainty, and taking into account the potential impact of actual, irregular inland topographies on long-term coastal change.

In this paper we present a cliff recession model which allows for realistic GSLR scenarios and inland topographies. First, the key variables, assumptions and parameters are introduced, and the model itself derived from mass conservation principles. The procedure for parameter estimation and incorporation of uncertainty into model predictions is detailed. The model is analyzed mathematically and the conditions for long-term system behavior (including equilibrium) found. Then, an algorithm suitable for application to real coastal profiles is described. Model predictions are compared to historical erosion on the Holderness coast, UK. We apply the model to representative profiles extracted from a compound Digital Elevation Model (DEM) of the Holderness coast and evaluate the timescale of both future equilibrium approach and typology change resulting from four different GSLR scenarios. The results of the model applications are discussed, the limitations of this work examined, and potential directions of future study identified.

2. Model Formulation

Here the model derivation is explained. Since the model has conceptual similarities with Wolinsky and Murray (2009), where the present equations have a direct analogue in the cited paper, this will be specified.

2.1. Schematic Representation of a Soft Cliffed Coast

A schematic representation of a transect of a soft cliffed coast is chosen, illustrated on Figure 1. Time is symbolized by t. The current cliff toe position is denoted $(x = x_c(t), y = y_c(t))$ where $x_c(t)$ is the horizontal position of the cliff toe, and $y_c(t)$ its elevation. The x-axis extends seawards perpendicular to the cliff toe, and the y-axis is vertical. $\frac{dx_c}{dt} < 0$ indicates a retreating coast. The x and y axes are assumed to be centered on the initial position of the cliff toe, so $x_c(t = 0) = 0$ and $y_c(t = 0) = 0$. The instantaneous sea level considered is the MLWL (Mean Low Water Level), see Figure 1. $R(t)$ is the rate of RSLR as a function of time. $R(t)$ is the sum of both GSLR and $VLM(t)$ (vertical land movement), which includes local changes in land elevation due to glacial isostatic adjustment (GIA) or tectonic processes. The beach profile has length L_s and depth H_s, and its end point is the point of closure. The cliff height at time t is denoted by $H_c(t)$ and the inland relief is denoted by $H(x)$, relative to $y = 0$.

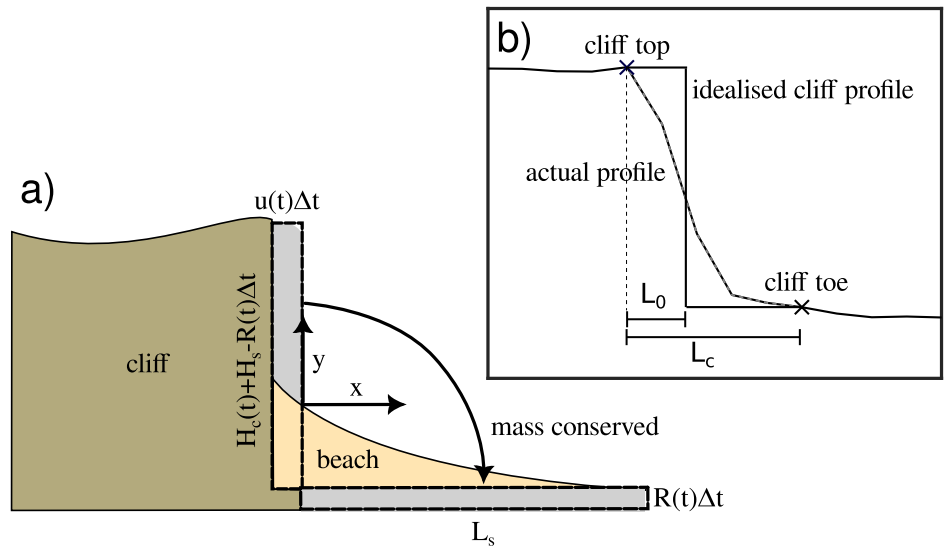

Figure 2. Panel (a) Cliff retreat over a small time step Δt. Dashed boxes indicate the volumes of sediment involved in the accommodation process. The cliff (darker brown) and beach (lighter brown) are shown. The volume of beach material necessary for accommodation is $L_s R(t)\Delta t$, and the volume eroded from the cliff is $(H_c(t) + H_s - R(t)\Delta t)\, u(t)\Delta t$. Panel (b) A realistic cliff with a horizontal distance of L_c between the cliff top and toe. This profile is approximated by a vertical cliff at a set horizontal distance L_0 between the top and toe. Figure created by the lead author. © University of Nottingham.

The cliff height as a function of time is then $H_c(t) = H(x_c(t)) - y_c(t)$. The cliff top slope $S(t)$ is equal to $-\frac{dH}{dx}$ calculated at $x = x_c(t)$.

c_b and c_c represent the sand concentration of the beach and cliff respectively, and express geological differences between the cliff material and the beach sediment. Hereinafter, we express these time-independent parameters through their ratio $\overline{c} = \frac{c_b}{c_c}$, which quantifies the relative volume of eroded cliff material which contributes to beach volume. By comparing the fraction of sand and gravel in cliff and beach material, $\overline{c}$ is expressed in terms of more easily measurable geological parameters (Hobbs et al., 2013; Román-Sierra et al., 2014) as

$$\overline{c} = \frac{c_b}{c_c} = \frac{1 - \phi_b}{s_f(1 - \phi_c)}, \tag{1}$$

where the cliff and beach porosities are ϕ_c and ϕ_b respectively, and the ratio of the volume of sand and gravel to the total volume of solid material in the cliff is s_f. The use of s_f assumes that fine clay and silt particles are washed away by wave action. We also assume that sands contained in the cliff and beach have the same density, meaning that mass is conserved in the model, not just volume of material.

To translate a real sloping cliff into the idealized representation in Figure 1, the cliff slope must be approximated by a vertical line, as shown in Figure 2b. The position of this vertical line relative to the cliff top and cliff toe must be chosen initially. We choose the center of mass of the roughly triangular cliff as the shoreline, since while the volume of material contained in the cliff is assumed to be negligible, this choice of shoreline minimizes the effect of this error. The sloping cliff (see Figure 2b) is roughly a right-angled triangle, with base L_c. Then, the horizontal position of the vertical cliff is chosen as $L_0 = (1 - \frac{1}{\sqrt{2}})L_c$ from the cliff top, such that the volumes of material between the cliff top and the vertical line, and the vertical line and the cliff toe are roughly equal. Also, we must assume the boundary between cliff and beach can be represented by a single point, the cliff toe. Cliff geology can be complex (Hobbs et al., 2013) and a cliff toe may not be well-defined on some coasts.

We derive a sediment conservation law as the cliff retreats. The timescale of study is in the hundreds to thousands of years, which affects the modeling assumptions. The key one is that the beach and cliff toe shift vertically at the same rate as the relative sea level rises, meaning $\frac{dy_c(t)}{dt} = R(t)$ (see Figure 1). This requires sediment, which comes exclusively from cliff retreat, illustrated in Figure 2a. Additionally, the beach has a constant equilibrium profile,

with fixed horizontal extent L_s between the cliff toe and closure point, and vertical extent H_s equal to the vertical distance between the cliff toe and the closure point. Closure depth is measured relative to MLWL(t) as in Hallermeier (1980), to account for tidal variation. $\overline{c}$ is assumed to be constant in time. All this amounts to an extension of the cliff retreat model explored by Wolinsky and Murray (2009), but now $R(t)$ and $S(t)$ are time-varying. This model assumes RSLR causes no feedback through changes in other sediment sinks or sources (Brooks & Spencer, 2012; Le Cozannet et al., 2014; Passeri et al., 2015).

2.2. Mass Conservation Equation

For a single infinitesimal time step Δt, the volume per unit width of sediment needed to support a beach which rises at the same rate as sea level is calculated, indicated in Figure 2a. The volume per unit width of sediment eroded from the cliff is also found and divided by $\overline{c}$ to get the volume of cliff material which contributes to the beach. The resulting volume (or mass) conservation equation is

$$-[H_c(t) + H_s - R(t)\Delta t]\, u(t)\Delta t = \overline{c} L_s R(t)\Delta t, \tag{2}$$

where $u(t) = \frac{dx_c}{dt} < 0$. Equation 2 is first divided by Δt, then by letting $\Delta t \to 0$,

$$-[H_c(t) + H_s]\, u(t) = \overline{c} L_s R(t). \tag{3}$$

We can apply the chain rule to find

$$\frac{dH}{dt} = \frac{dH}{dx}[x_c(t)]\, \frac{dx_c}{dt}(t) = -S(t)u(t). \tag{4}$$

The relationship $H_c(t) = H(x_c(t)) - y_c(t)$, is combined with the relationship $\frac{dy_c(t)}{dt} = R(t)$ and Equation 4 to give

$$\frac{dH_c(t)}{dt} = -[S(t)u(t) + R(t)]. \tag{5}$$

Note that Equation 3 is analogous to Equation 10 in Wolinsky and Murray (2009), where here $R(t)$ and $S(t)$ is considered time-varying.

Equation 3 can be written in terms of $H_c(t)$, and then differentiated with respect to t to give

$$\frac{dH_c(t)}{dt} = -\frac{\overline{c} L_s \left[\frac{dR}{dt} u(t) - R(t)\frac{du}{dt}\right]}{u^2(t)}. \tag{6}$$

Equations 5 and 6 are combined to obtain a first-order ordinary differential equation in terms of $u(t)$:

$$\frac{du(t)}{dt} = \frac{1}{R(t)}\frac{dR(t)}{dt}u(t) - \frac{1}{\overline{c} L_s}u(t)^2 - \frac{S(t)}{\overline{c} L_s R(t)}u(t)^3. \tag{7}$$

Equation 7 is our model, relating cliff retreat rate $u(t)$ to $R(t)$ and $S(t)$. This is a generalization of Equation 13a in Wolinsky and Murray (2009) for time varying $R(t)$ and $S(t)$. Also, note that Equation 5 is analogous to Equation 12 in Wolinsky and Murray (2009).

2.3. Parameter Estimation

The values of six parameters are needed to apply Equation 7. The values of $GSL(t)$ (global sea level), DoC (morphodynamic depth of closure), $VLM(t)$ (total vertical land movement), $MLWL(t = 0)$ (initial mean low water level), H_t (initial cliff toe elevation relative to Ordnance Datum Newlyn, ODN) and $\overline{c}$ are chosen as a best guess using evidence from other literature. $GSL(t)$ and $VLM(t)$ can be obtained from field observations such as tidal gauge data (Jevrejeva et al., 2014), geological records (Lambeck et al., 2014), satellite scanning (Ivins & Wolf, 2008; Jevrejeva et al., 2014) and modeling (Clark et al., 2016; Whitehouse, 2018).

A value for DoC is necessary to estimate H_s. One method for calculating this is the timescale dependent formula (Birkemeier, 1985; Nicholls et al., 1998):

$$DoC = 1.75\mathcal{H}_\tau - 57.9\frac{\mathcal{H}_\tau^2}{gT_\tau^2}, \tag{8}$$

where g is the acceleration due to gravity (assumed equal to 9.81 m/s^2), $\mathcal{H}_\tau$ is the non-breaking significant wave height (SWH) exceeded for 12 hr in the study duration τ and T_τ is the associated wave period. There is little consensus on the best choice of DoC for use in coastal models, and many formulae are available in the literature, but Equation 8 is cited by Shand et al. (2013) as providing a mid-range estimate of shoreline retreat. We apply this formula to a representative study timescale of 1,000 years, assuming that the wave climate is stationary over the modeling duration. However, we acknowledge that Equation 8 was developed for shorter timescales than our study duration, which means that it is used beyond its validated timescale of years to decades (Ortiz & Ashton, 2016). We fit a Generalized Pareto Distribution (GPD) to the tail of a sample SWH distribution using maximum likelihood estimation (Teixeira et al., 2018), using a threshold of 95%. The percentile q of the statistical distribution of the sample corresponding to the value of $\mathcal{H}_\tau$ is:

$$q = 100\left(1 - \frac{12}{\tau}\right), \tag{9}$$

where τ is the representative timescale of the study, measured in hours. The corresponding percentile for $\tau = 8,766,000$ hr (i.e., 1,000 years in hours), is $q = 99.999863$. We then use the inverse cdf (cumulative distribution function) of the GPD to find $\mathcal{H}_{1000yr}$ from q.

The other value necessary for the calculation of DoC is an estimate of T_{1000yr}. This is obtained by looking at the mean periods of the largest significant wave heights in the sample and letting T_{1000yr} lie at the higher end of these extreme periods, since mean wave period tends to scale with SWH (Holthuijsen, 2010). An upper bound for the ratio between wave height and water depth is around 0.88 (Bosboom & Stive, 2021). This physical limit is used to check whether a wave with height $\mathcal{H}_{1000yr}$ would break at the closure point.

Determining $MLWL(t = 0)$ requires detailed historical data which may not exist for a specific location. An estimate involving the averaging of tidal gauge data close to the study site, is used here. We calculate $\bar{c}$ with Equation 1. Since representative values of ϕ_b, ϕ_c and s_f are likely to have been estimated for an area of interest.

2.4. Introducing Uncertainty on Future RSLR

GSLR projections from the year 2,000 to 12,000 by Clark et al. (2016) are used in this work, and they are shown in Figure 3. They are generated considering four scenarios of carbon emissions, numbered from 1 to 4, corresponding to 1,280, 2,560, 3,840, 5,120 gigatonnes of carbon (GtC) released between the years of 2000 and 2300, peaking in 2100, respectively.

3. Model Analysis

3.1. Analytical Solutions of the Model With Constant S

We introduce the non-dimensional rate of recession $v(t)$, where

$$v(t) = -\frac{u(t)}{R(t)}. \tag{10}$$

$v(t)$ is positive, and expresses the cliff recession per unit RSLR. If $S(t)$ is constant ($S(t) = S_0$), Equation 7 has an analytical solution, derived in Appendix A, even if $R(t)$ is variable:

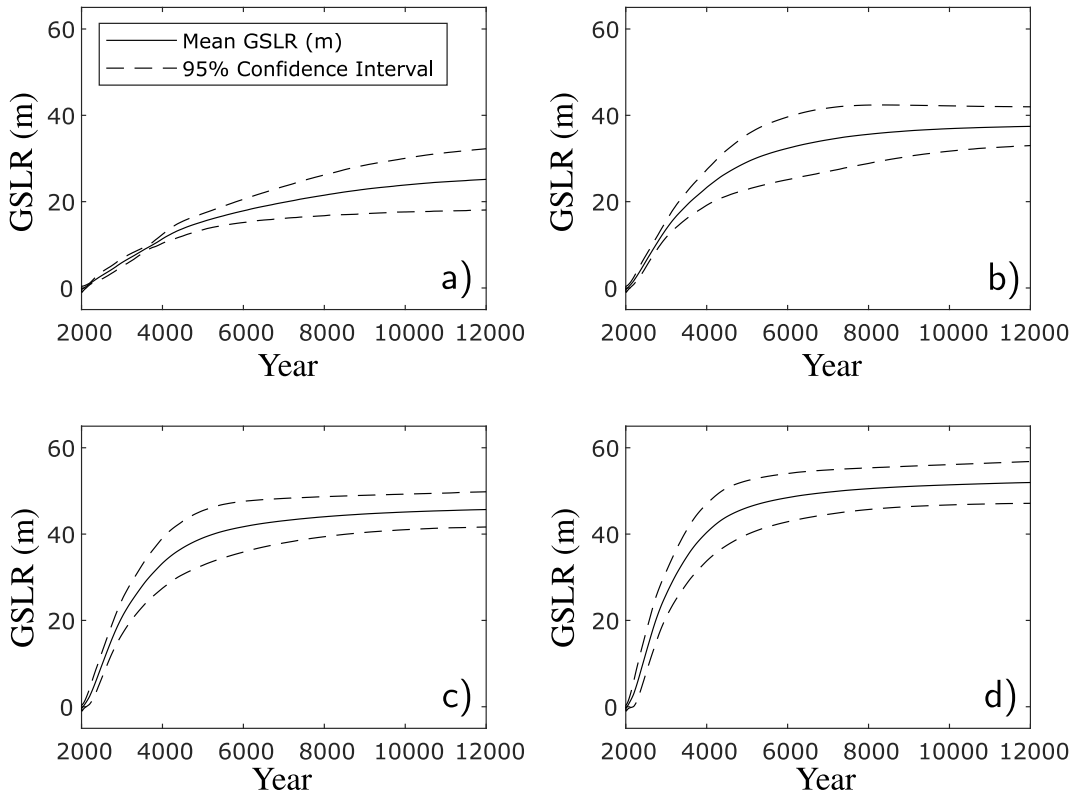

Figure 3. The GSLR projections from Clark et al. (2016), with the mean predicted change in sea level from the year 2000 (solid line), and the 95% confidence intervals for these predictions included (dashed lines). Panels (a–d) show Scenarios 1 to 4 respectively. Figure created by the lead author. © University of Nottingham.

$$v(t) = \begin{cases} \dfrac{1}{S_0\left[W_0\left(a_1 \exp\left[\dfrac{P(t)}{\bar{c}L_s S_0}\right]\right)+1\right]} & S_0 > 0 \\ \dfrac{\bar{c}L_s}{H_s + H_c(t=0) - P(t)} & S_0 = 0 \\ \dfrac{1}{S_0\left[W_{-1}\left(a_1 \exp\left[-\dfrac{P(t)}{\bar{c}L_s S_0}\right]\right)+1\right]} & S_0 < 0. \end{cases} \tag{11}$$

Here $P(t) = \int_0^t R(\rho)d\rho$, is the cumulative RSLR between $t = 0$ and time t (introducing ρ as a dummy variable). It is worth noting that $R(t) = \frac{dP}{dt}$, which will be useful when finding the analytical solution for x_c (Equation 15). The Lambert W function (Corless et al., 1996) used in this solution is defined implicitly as

$$W(x)\exp(W(x)) = x, \quad x \geq -\frac{1}{e}, \tag{12}$$

where x is a generic variable. We can use this to get an expression for $H_c(t)$, by substituting Equation 11 into Equation 3:

$$H_c(t) = \begin{cases} \overline{c}L_s S_0 \left[W_0\left(a_1 \exp\left[-\frac{P(t)}{\overline{c}L_s S_0} \right] \right) + 1 \right] - H_s & S_0 > 0 \\ H_c(t=0) - P(t) & S_0 = 0 \\ \overline{c}L_s S_0 \left[W_{-1}\left(a_1 \exp\left[-\frac{P(t)}{\overline{c}L_s S_0} \right] \right) + 1 \right] - H_s & S_0 < 0. \end{cases} \quad (13)$$

This differs from Equation 14 of Wolinsky and Murray (2009) for $H_c(t)$ since $R(t)$ is time-varying, and $H_c(t)$ is written explicitly as a function of the total RSLR. $H_c(t)$ at any time depends on $P(t)$, not on t itself, therefore it is path-independent. The constant a_1, by substituting $P(t) = 0$ into Equation 13, is

$$a_1 = \left[\frac{H_c(t=0) + H_s}{\overline{c}L_s S_0} - 1 \right] \exp\left[\frac{H_c(t=0) + H_s}{\overline{c}L_s S_0} - 1 \right]. \quad (14)$$

One crucial point is that the Lambert W function defined on the real numbers is multi-valued, with an principal branch W_0, and secondary branch W_{-1}. In Appendix B we show that the solution cannot switch branches, and the two branches can be treated as two individual functions. We now continue with finding the analytical solution, solving to find the cliff toe position $x_c(t)$. The derivation of the following is detailed in Appendix C:

$$x_c(P) = \begin{cases} \overline{c}L_s \ln\left[\frac{W_0\left(a_1 \exp\left[-\frac{P}{\overline{c}L_s S_0} \right] \right)}{W_0(a_1)} \right] & S_0 > 0 \\ \overline{c}L_s \ln\left[1 - \frac{P}{H_c(t=0) + H_s} \right] & S_0 = 0 \\ \overline{c}L_s \ln\left[\frac{W_{-1}\left(a_1 \exp\left[-\frac{P}{\overline{c}L_s S_0} \right] \right)}{W_0(a_1)} \right] & S_0 < 0, \end{cases} \quad (15)$$

taking into account that $a_2 = -\overline{c}L_s \ln|W(a_1)|$, and logarithms can be combined. The absolute value function is dropped, since the signs of $W(a_1)$ and $W\left(a_1 \exp\left(-\frac{P}{\overline{c}L_s S_0}\right)\right)$ are equal, so the quantity inside the logarithm is always positive. A computational consideration is that for S_0 very close to zero, a_1 exceeds the maximum value which some programming languages (we used MATLAB in this work) can handle. Therefore if $\ln|S_0| < -11$, small enough to cause numerical errors, we assume the slope is equal to zero, since any effects on model output will be negligible.

This analytical solution shows that the total retreat $x_c(P)$ depends only on the change in sea level over the whole study duration, and is independent of the intermediate values of $R(t)$. This extends to all topographies formed of straight line segments. The dependence of x_c on P only means that the year-to-year uncertainty in GSLR projections does not directly affect model predictions, and only the uncertainty in final relative sea level change needs to be considered.

Equation 15 is inverted, so the RSLR needed for a cliff to erode through a section of inland with constant slope is calculated:

$$P(x_c) = \begin{cases} [H_c(t=0) + H_s]\left[1 - \exp\left(\frac{x_c}{\overline{c}L_s} \right) \right] & S_0 = 0 \\ -S_0 x_c + [H_c(t=0) + H_s - \overline{c}L_s S_0]\left[1 - \exp\left(\frac{x_c}{\overline{c}L_s} \right) \right] & S_0 \neq 0. \end{cases} \quad (16)$$

The critical RSLR P_c for which cliff height reaches zero can be obtained. This is necessary for analysis of the time of coastal typology change. We find this by letting $H_c(t) = 0$ in Equation 13, and rearranging for P:

$$P_c = \begin{cases} H_c(t=0) & S_0 = 0 \\ H_c(t=0) - \overline{c}L_s S_0 \ln\left[\dfrac{H_s - \overline{c}L_s S_0}{H_c(t=0) + H_s - \overline{c}L_s S_0}\right] & S_0 \neq 0. \end{cases} \quad (17)$$

When inland topographies are approximated by a series of straight line segments, the sea level rise needed to erode through each region of constant slope can be calculated with Equation 16. The region of constant slope the cliff retreats into for a given P can then be identified, and the retreat driven by the remaining RSLR can be calculated with Equation 15, giving a value for $x_c(P)$. We can calculate the RSLR necessary for model breakdown in a similar way: Equation 16 is used to find the line segment the cliff toe touches when cliff height reaches zero, and Equation 17 finds the RSLR necessary for typology change. Equations 16 and 17 provide an elegant and computationally efficient first-estimate for the timescale of cliff submergence, useful for identifying vulnerable areas, and guiding further modeling studies.

3.2. Long-Term Behaviors Predicted by the Model

The analytical solution for $v(t)$ and $H_c(t)$ in the case of $S = S_0$ and time-varying $R(t)$ (Equations 11 and 13 respectively) are here used to analyze the long-term behavior of the system. Assuming $P(t)$ is a strictly increasing function, then if $S_0 \leq 0$, $H_c(t)$ (Equation 13) eventually becomes non-positive. At this point the model computation stops, since there is no cliff. However, if $S_0 > 0$, $H_c(t)$ approaches an constant equilibrium value H_{eq}, defined as

$$H_{eq} = \overline{c}L_s S_0 - H_s, \quad (18)$$

also discussed in Wolinsky and Murray (2009) (Equation 13b). If H_{eq} is positive, then equilibrium cliff height would be reached before model breakdown. We define S_c as

$$S_c = \frac{H_s}{\overline{c}L_s}, \quad (19)$$

which differentiates between different long-term behaviors. If $S_0 < S_c$, the cliff height reaches zero in finite time. If $S_0 \geq S_c$, then a positive equilibrium cliff height is approached asymptotically. For an equilibrium cliff profile to form, the backshore slope must be greater than the average shoreface slope, with adjustment for substrate composition. As equilibrium is approached, v approaches the dimensionless equilibrium rate of retreat v_{eq}, where

$$v_{eq} = \frac{1}{S_0}, \quad (20)$$

consistent with Wolinsky and Murray (2009). The equilibrium dynamics of Equation 7 are summarized showing v as a function of P (Figure 4a).

A non-positive cliff height occurs if and only if $v(t)$ is faster than some critical rate v_c, which can be deduced from setting $H_c = 0$ in Equation 3. The constraints on $v(t)$ are expressed mathematically as

$$0 < v(t) < \frac{\overline{c}L_s}{H_s}, \quad (21)$$

therefore, $v_c = \frac{\overline{c}L_s}{H_s}$, shown on Figure 4a. H_{eq} is only achieved in certain conditions, controlled by the value of S_0. We can interpret this behavior physically. If $S_0 \geq S_c$, v approaches v_{eq} as P increases, and no typology change occurs. For $S_0 < S_c$, v will increase with P until a critical value $v = v_c$ where typology change occurs. The case $0 < S_0 < S_c$ (Figure 4b) differs from $S_0 \leq 0$ (Figure 4c) physically since a negative slope is likely to lead to an overwash scenario after the cliff is submerged. With a positive slope, it seems more likely that a different, stable coastal type, such as a barrier beach (Murray & Moore, 2018), would form.

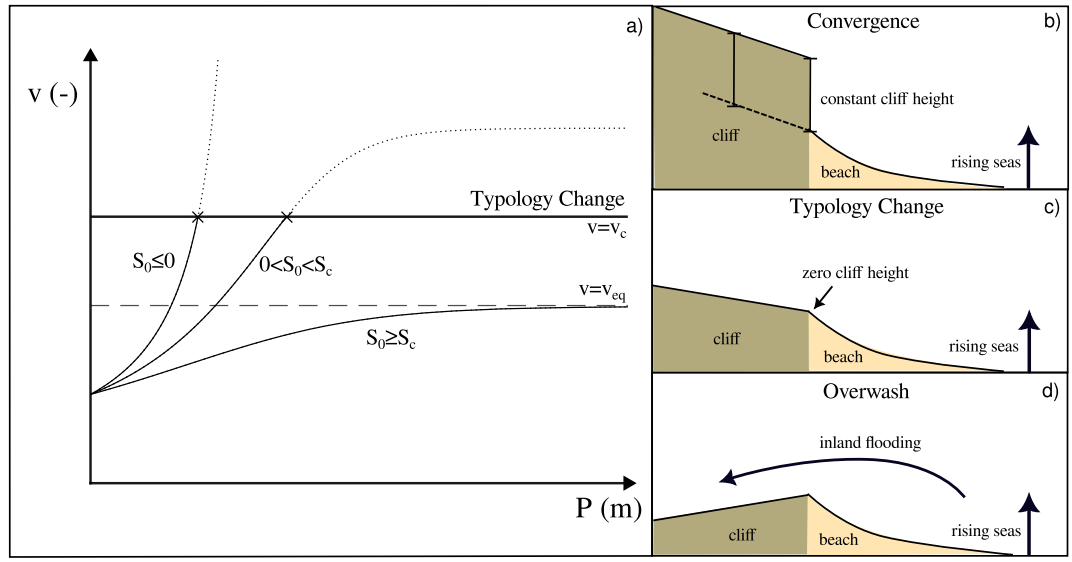

Figure 4. Panel (a) the equilibrium dynamics of a system evolving according to Equation 7 in terms of v (the non-dimensional retreat rate) as a function of P (total RSLR). For $S_0 \geq S_c$, v approaches an equilibrium value as sea level rises. Otherwise, typology change occurs. Panels (b, c and d) show the three possible long-term behaviors predicted by the model. Panel (b) Equilibrium behavior, where the H_c and v approach constant values. Panel (c) Non-equilibrium behavior in the case of $0 < S_0 < S_c$. Panel (d) an overwash scenario, where $S_0 \leq 0$. Figure created by the lead author. © University of Nottingham.

3.3. Total RSLR Required for Equilibrium Approach

The equilibrium cliff height is not reached in finite time, from Equation 13, so the concept of a half-life is adapted and used to estimate the RSLR needed for the cliff height to be half as far from its equilibrium value. Since $H_c(t)$ is a function of relative sea level change only (as shown in Equation 13), we define $P_{\frac{1}{2}}$ as the RSLR required for $H_c(t)$ to change from its initial value to the midpoint between its initial value and the equilibrium value. We approximate Equation 13 for $S_0 > 0$ with an exponentially decaying function:

$$H_{eq} + A\exp(-\lambda F) \approx \bar{c}L_s S_0\left[W_0\left(a_1 \exp\left[-\frac{P(t)}{\bar{c}L_s S_0}\right]\right) + 1\right] - H_s, \tag{22}$$

where λ is the decay constant. We assume the cliff height is approximately at equilibrium, meaning $a_1 \exp\left(-\frac{P(t)}{\bar{c}L_s S_0}\right)$ is approximately zero. Then we can use the Taylor series expansion of the Lambert W function: $W_0(x) \approx x$ when x is small. Therefore:

$$H_{eq} + A\exp(-\lambda F) \approx \bar{c}L_s S_0 - H_s + \bar{c}L_s S_0 a_1 \exp\left[-\frac{P(t)}{\bar{c}L_s S_0}\right], \tag{23}$$

and we can approximate $\lambda = \frac{1}{\bar{c}L_s S_0} = \frac{1}{H_{eq}+H_s}$. We can use the formula $P_{\frac{1}{2}} = \frac{\ln 2}{\lambda}$ and calculate:

$$P_{\frac{1}{2}} \approx \ln(2)(H_{eq} + H_s) \approx \ln(2)[H_c(t=0) + H_s]. \tag{24}$$

Global sea level has risen by around 130 m since the end of the last ice age (Clark et al., 2016). If $P_{\frac{1}{2}}$ for a cliff is much less than this, then many cliffs which can achieve equilibrium due to their value of S_0 (sufficiently steep and approximately constant) are close to this equilibrium. Also, shorter cliffs approach this equilibrium more quickly than taller ones. This timescale of equilibrium approach is of a similar magnitude to that found by Wolinsky and Murray (2009).

3.4. Probability of Typology Change

The uncertainty in GSLR projections is included in the modeling of the cliffed coast evolution. The modeled recession distance depends on total RSLR, so to find the mean and 95% confidence bounds for cliff recession, we need only to use the mean and 95% confidence bounds for GSLR as model inputs. We ignore negative relative sea level change, since this is beyond the scope of the model. The RSLR necessary for typology change is independent of the GSLR scenario, and is denoted by P_c. The probability that transition occurs before time T is equal to $\mathbf{P}(P_c < P(T))$.

$$\mathbf{P}(P_c < P(T)) = \frac{1 - \Phi\left(\frac{P_c - \mu_t + VLM(t)}{\sigma_t}\right)}{1 - \Phi\left(\frac{-\mu_t + VLM(t)}{\sigma_t}\right)}, \tag{25}$$

where μ_t and σ_t are the mean and standard deviation of the global sea level and Φ is the cumulative distribution function (cdf) of the standard normal distribution. The denominator is a correction factor assuming that relative sea level cannot decrease.

4. Application to the Holderness Coast, U.K

4.1. Modeling Future RSLR-Driven Erosion of the Holderness Coast

We now apply the model to the Holderness Coast, East Yorkshire, U.K. (see Figure 5a). This is a stretch of coast delimited to the north by Flamborough Head and by Spurn Head to the south (Figure 5a). Soft cliffs composed of glacial till occur along the whole coast, their erosion is driven by marine (waves, sea level) action and the instability of the cliffs due to seepage (Brown et al., 2012). The rapid retreat of these soft cliffs results in one of the fastest eroding coastlines in Europe, as such it has been widely studied and monitored; the reader is referred to Brown et al. (2012) for a literature review on the subject.

4.1.1. Future GSLR

The four previously discussed carbon emissions scenarios from Clark et al. (2016) are used to predict both changes in cliff recession rates and typology changes. In these projections, for the first few decades modeled, global sea level decreases slightly before increasing, which we believe corresponds to the spin-up period of GSLR model of Clark et al. (2016), rather than being a genuine prediction for this time interval. After 100 years, the general trend of sea level rise is established in these projections. We therefore begin our simulations at the year 2100.

4.1.2. Waves

A time series of SWH and peak period is necessary to estimate the depth of closure. The hourly significant height of wind waves and mean wave period are extracted from the ERA5 atmospheric reanalysis (Hersbach et al., 2023) of global climate at the $54°N, 0°E$ point, offshore of the Holderness coast. These time series are selected to span a total of 42 years, from 1 January 1980 to 31 December 2021, since this is a time interval supported by the assimilation of tidal gauge and remote sensing data.

4.1.3. Selected Transects

Modeling of cliffed coast evolution is carried out at 11 locations representative of the variability of coastal features along the Holderness coast (Figure 5b). These are extracted from a composite Digital Elevation Model (DEM) comprising three individual DEMs. The 2019 SurfZone DEM (resolution 2 m) combines LiDAR (Light Detection and Ranging) and multibeam SONAR (Sound Navigation And Ranging) scans of the topography and bathymetry close to the Great Britain coastline, creating a seamless DEM of the intertidal zone (Environment Agency, U.K., 2019). The SurfZone DEM extends about 1 km offshore, which may not reach closure depth, and about 1 km inland, which may be traversed by an eroding cliff over the timescale of interest. Therefore, we need to augment the SurfZone DEM, both inland and offshore, using additional topography and bathymetry DEMs. The OceanWise DEM (resolution 1 arc s) generated by single and multibeam echo sounding is used for bathymetry (OceanWise, 2020). The topography used is the 2022 LiDAR composite DEM (resolution 10 m) from the

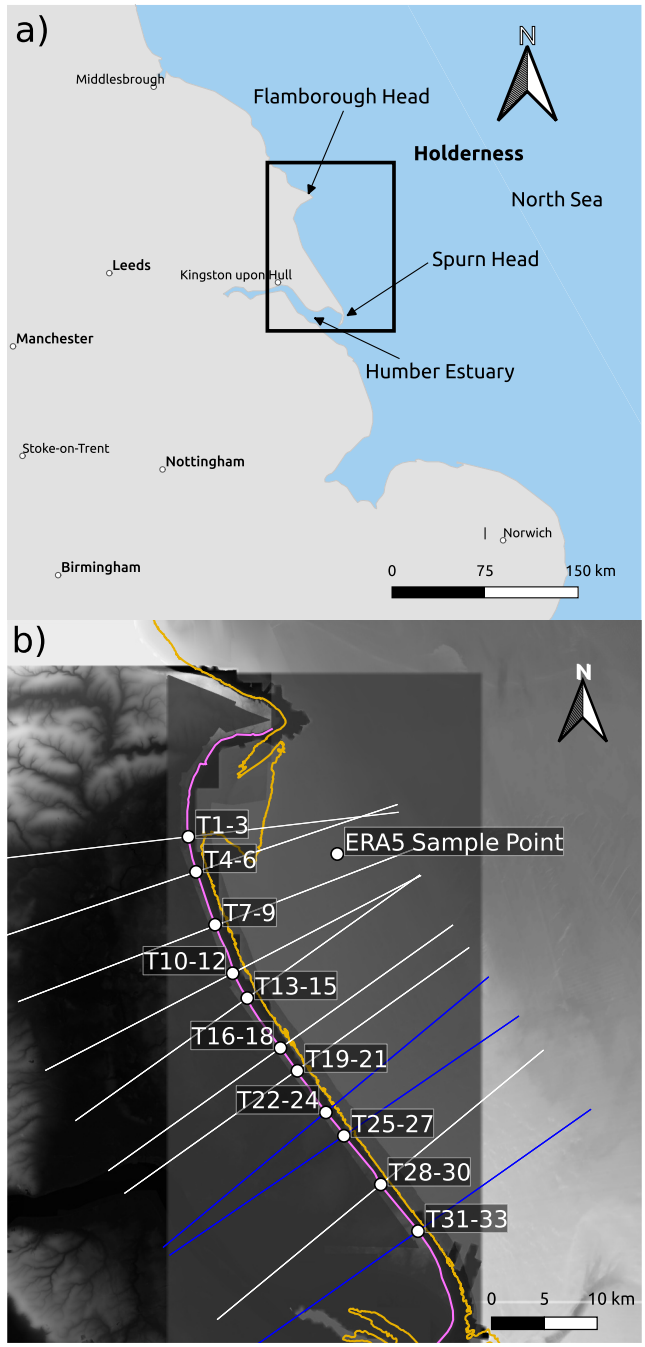

Figure 5. Panel (a) The location of the Holderness coast in the UK, highlighted by the black box. The coast stretches from Flamborough Head in the North to Spurn Head and the Humber estuary to the South. Panel (b) The geographic context of the transects T1-33 (white and blue) extracted from the 11 locations along Holderness coast (labeled white dots). The blue transects are those further discussed when the effects of future RSLR scenarios on the Holderness coast are modeled. The three DEMs shown: the high resolution SurfZone DEM close to the 0 m shoreline (pink line), the bathymetry extending eastwards, and the topography stretching westwards. The location of the ERA5 node from which wave conditions are sampled is also indicated with a white circle. The closure contour used in the model (yellow) is relative to a MLWL of −1.78 m (ODN), with $DoC = 9.77$ m.

Environment Agency, U.K. (2022). The bathymetry is shifted vertically upwards by 3.33 m (since the bathymetry is referenced to Chart Datum (CD) and the topography and SurfZone DEMs are referenced to ODN). When profiles are created, the higher resolution SurfZone DEM is taken as the main DEM, and then bathymetry and topographic data are used to fill areas inland and offshore, beyond its spatial extent. The 0 m contour of the SurfZone DEM is extracted and smoothed using the Ramer–Douglas–Peucker algorithm (distance dimension 50 m) (Visvalingam & Whyatt, 1990). Three transects perpendicular to this smoothed contour 10 m apart, were created for each location using the QGIS transects tool. These stretch 20 km inland and seaward, reaching the closure contour for all profiles.

4.1.4. Historical Rates of Retreat on the Holderness Coast

Prior to modeling the effect of future RSLR, we compare modeled cliff retreat driven by relative sea level rise (RSLR) with observed cliff retreat over a long time period. Since we cannot isolate the portion of retreat attributable to RSLR on this coast directly from observation, we aim only to provide an order-of-magnitude estimate of the cliff retreat required to balance the sediment demands created by RSLR-driven accommodation.

We compare modeling results to estimated rates of retreat on the Holderness coast covering the period from 1852 to 2005. This data is from Brown et al. (2012), extracted from historical maps. During this time, relative sea level rose by an estimated 32.2 cm, comprising 7.65 cm of glacial isostatic adjustment (Stockamp et al., 2015) and 24.58 cm of global sea level rise (GSLR) (Jevrejeva et al., 2014). We assume that wave climate and cliff composition have remained consistent throughout this validation period. The topography of the eroded area is unknown, but it is assumed that the eroded topography would be similar enough to the current topography that the transects indicated in Figure 5 can be substituted in for an order of magnitude estimate.

4.1.5. Additional Parameter Estimates

To estimate future wave conditions, we assume the future wave climate is stationary, and use historical data (ERA5 wave climate time series) to estimate DoC. Fitting the largest 5% of wave heights with a GPD and finding the 99.999863th percentile finds $\mathcal{H}_{1000yr} = 6.61$ m. The water depth at $54°N, 0°E$ is 24.7 m, approximately relative to ODN. The ratio of this wave height to the water depth is therefore about 0.268, not close to the breaking limit (Riedel & Byrne, 1987), and therefore physically plausible. The largest wave in the record is 5.73 m, so estimation of T_{1000yr} requires extrapolation. The largest waves in the sample (those over 5 m high) have a peak period between 8.6 and 12.0 s, so we assume that a 6.61 m high wave would be at the higher end of this scale, and let $T_{1000yr} = 12$ s. Using Equation 8 estimates DoC as 9.77 m.

On the Holderness coast, most vertical land movement is attributed to GIA. The scientific consensus on rates of GIA across the UK is summarized in Stockamp et al. (2015), and a number of sources (geological records, geodetic measurement, mathematical modeling) indicate the Holderness coast is subsiding at a rate of $0 - 1$ mm/year. For the purposes of this study, we assume that $VLM(t) = -0.5$ mm/year. In reality, GIA may change over time if post-glacial rebound approaches an equilibrium.

The initial MLWL, calculated for the year 2000 (the start of the modeled future GSLR) is calculated as follows. The two closest tidal gauge sites with publicly available data (National Tidal and Sea Level Facility, 2024) are Immingham and Whitby. The spring and neap MLWLs predicted for 2008–2026 are averaged to get a general MLWL for each location. These are then transformed into ODN from local chart datum, and averaged between chart locations to estimate $MLWL$ in the year 2017. A correction of −54 mm is applied to reflect GSLR between 2000 and 2017, meaning $MLWL(t = 0) = -1.78$ m.

H_t is estimated for each of the 33 extracted transects, and the average value across the whole coast is 3.15 m. There is some ambiguity in the identification of the cliff toe: the presence of a talus may obscure its actual location, and the similarity in composition between the cliff and beach means a clear boundary may not exist. For the purposes of this study the cliff toe is chosen as the point on the cliff face with distinctly discontinuous gradient, indicating the intersection between cliff and beach. For each location, the cliff toe is identified manually on each of the three parallel transects, and the mean elevation used as H_t.

ϕ_c, ϕ_b and s_f vary locally, and the layering of glacial tills with other deposits mean finding representative values for a cliff section can be complex. Two dominant tills, the Skipsea and Withernsea tills (Bell, 2002), are chosen to

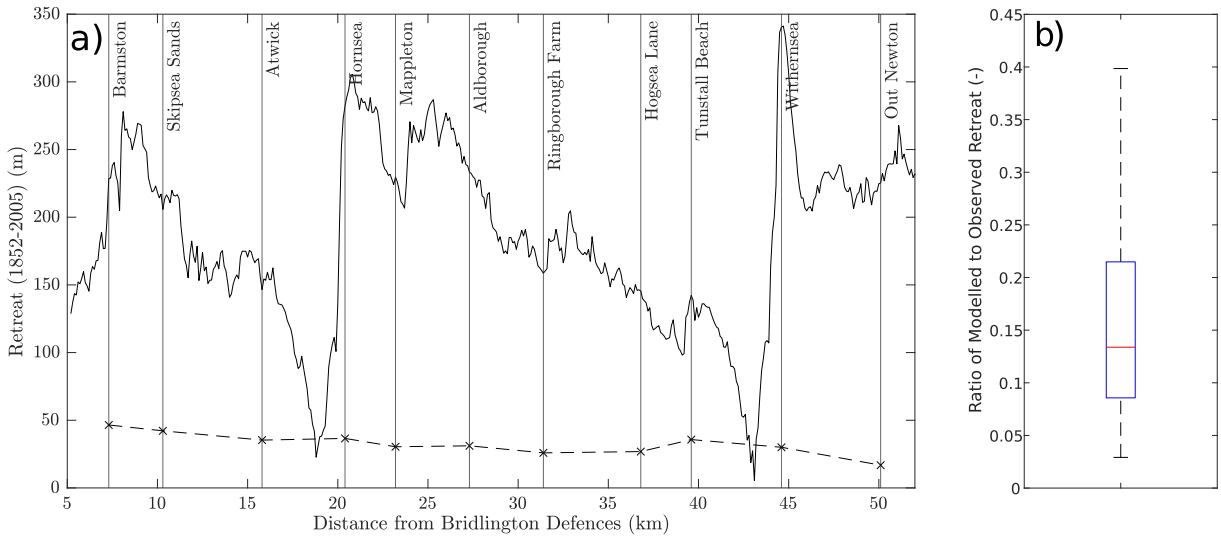

Figure 6. Panel (a) compares observed (solid black line, from (Brown et. al., 2012)) and modeled (dashed black line) retreat between 1852 and 2005. The box plot in panel (b) shows the variation of the ratio between modeled and observed retreat, with the median (red line), first and third quartile (blue box) and full range (black dashed line) indicated. The parts of the coast close to the Hornsea and Withernsea coastal defenses are omitted. Figure created by the lead author. © University of Nottingham.

represent the sand and gravel yield of the full coast, and therefore s_f is estimated as 0.31 (Pringle, 1985). Alternate estimates for s_f exist (Bell, 2002; Bell & Forster, 1991; Brown et al., 2012). ϕ_b and ϕ_c also vary, but 0.4 is considered a sufficient estimate for ϕ_b (Román-Sierra et al., 2014) and 0.25 for ϕ_c, assuming the cliff consists mainly of unoxidized till (Klinck et al., 1997). Equation 1 yields $\overline{c} = 2.58$.

5. Results of the Application to the Holderness Coast

5.1. Modeling Historical Cliff Retreat

The model is applied to three transects at each of the 11 locations (see Figure 5), and the averaged results are compared to observed retreat over the same period. Figure 6a presents the modeled retreat alongside the observed retreat, while Figure 6b displays a box plot of the ratio of modeled to observed retreat, offering an indication of the proportion of historical retreat driven by sea level rise. Modeled retreat values are interpolated between sampled locations. We exclude sections of the cliff near the coastal defenses at Hornsea and Withernsea, since human interventions are not considered in this model.

Our results suggest that, on average, approximately 13.4% of the observed retreat can be attributed directly to sea level rise. This implies that 86.6% of the sediment released by cliff erosion does not directly contribute to offsetting RSLR sediment demands but is instead likely transported into the Humber Estuary or dispersed offshore. However, there is considerable variability, with the lower quartile at 8.6% and the upper quartile at 21.5%.

5.2. Future Retreat

We show the results of model application for three representative transects, namely T23 (Hogsea Lane), T26 (Tunstall Beach), and T32 (Out Newton), which show various possible effects of GSLR. Figure 7 shows cliff retreat with uncertainty bounds at each location under each GSLR scenario. Typology change occurs for all three transects within the next 4,000 years. The retreat distances $|x_c(t)|$ (independent of GSLR scenario) corresponding to a change in typology are 1,941, 296, and 896 m for T23, T26, and T32, respectively. Excluding the most conservative GSLR scenario, acceleration in cliff recession is predicted at all three locations. Note the difference in axes limits in Figure 7, due to the very different $|x_c(t)|$ required for the onset of typology change.

Figure 8 shows both the probability density functions, calculated from Equation 25, for the year when typology change occurs, and the median year, at each location, for each scenario. For all transects the onset of the transition occurs progressively earlier from Scenario 1 to Scenario 4, as expected. However, the timescale of these transitions varies on the order of thousands of years among the transects, depending on both the initial H_c and the

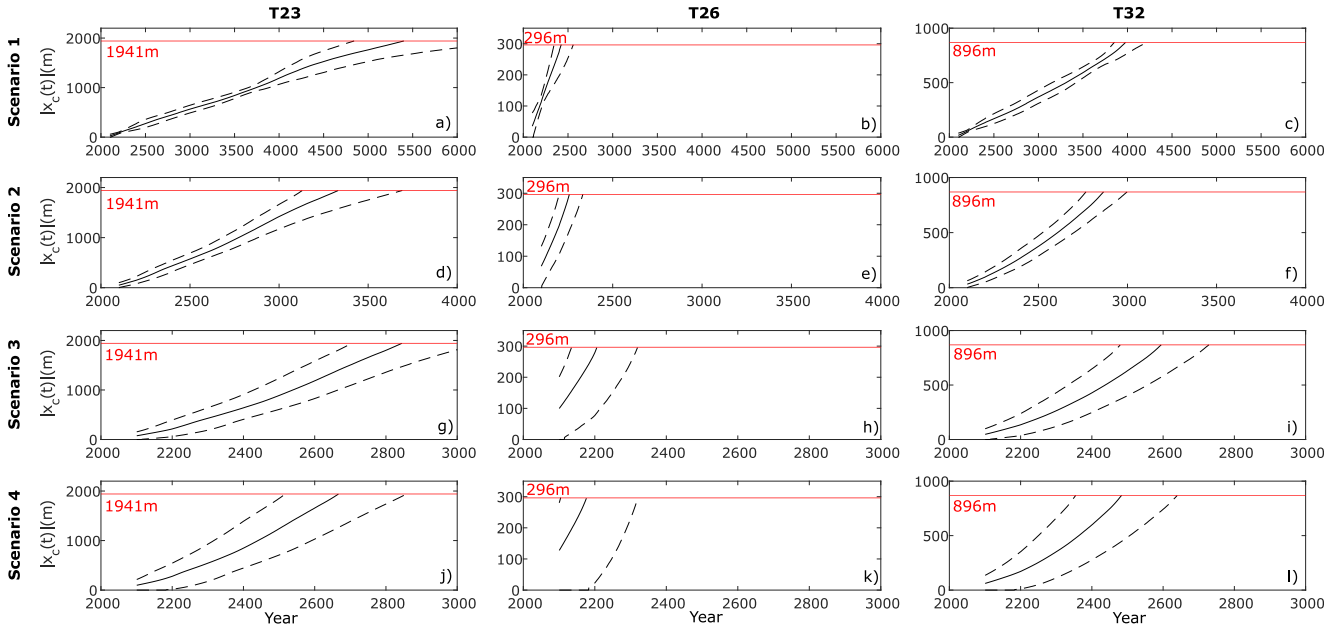

Figure 7. The mean (solid line) and 95% confidence bounds (dashed lines) for total cliff recession as a function of time according to the model. Four GSLR scenarios (Clark et al., 2016) are applied to three locations on the Holderness coast: Hogsea Lane (T23), Tunstall Beach (T26) and Out Newton (T32). The total cliff retreat where typology change occurs is indicated in red. Figure created by the lead author. © University of Nottingham.

inland topography. T26 is particularly vulnerable to a transition, predicted to occur between the years of 2178 and 2426, on average.

Figure 9 illustrates the influence of topography on retreat rate. Initially, H_c for T23, T26, and T32 are 15.9, 4.1, and 20.7 m, respectively. Increases in H_c correspond to decreases in non-dimensional retreat rate v, and vice versa.

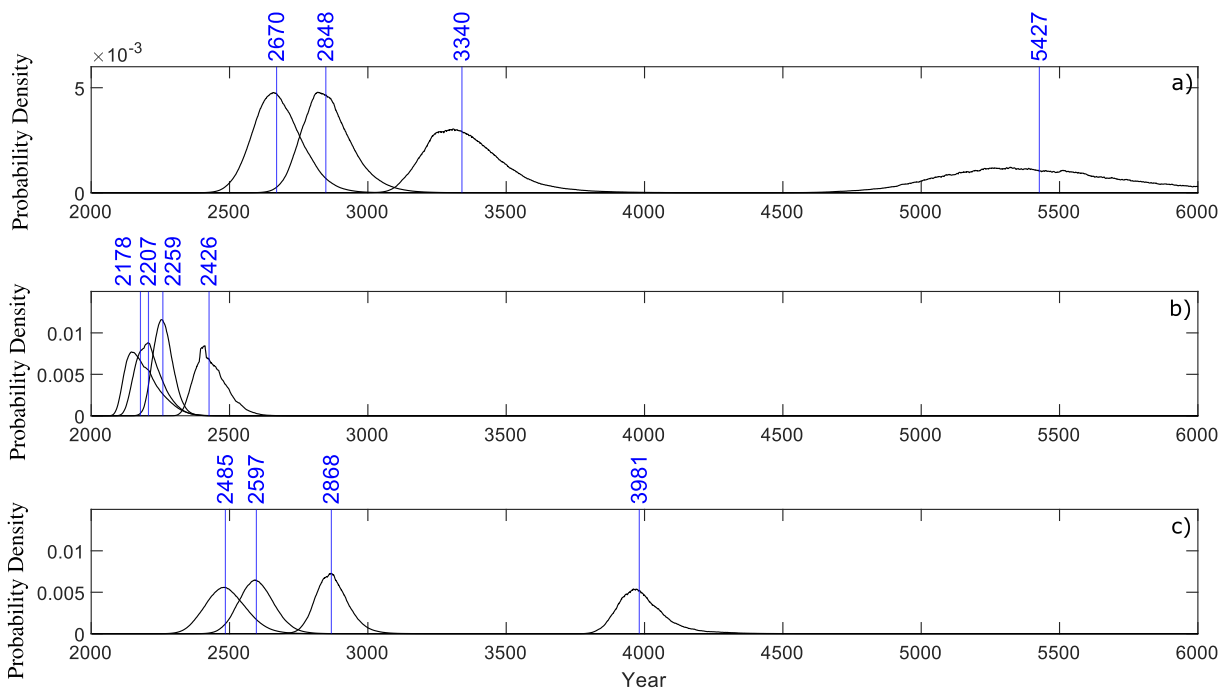

Figure 8. The probability distributions of the years of typology change for each of the four GSLR scenarios applied to the three chosen transects. Panel (a), T23, (b) T26, (c) T32. The median year of transition is indicated for each scenario with a labeled vertical line. Figure created by the lead author. © University of Nottingham.

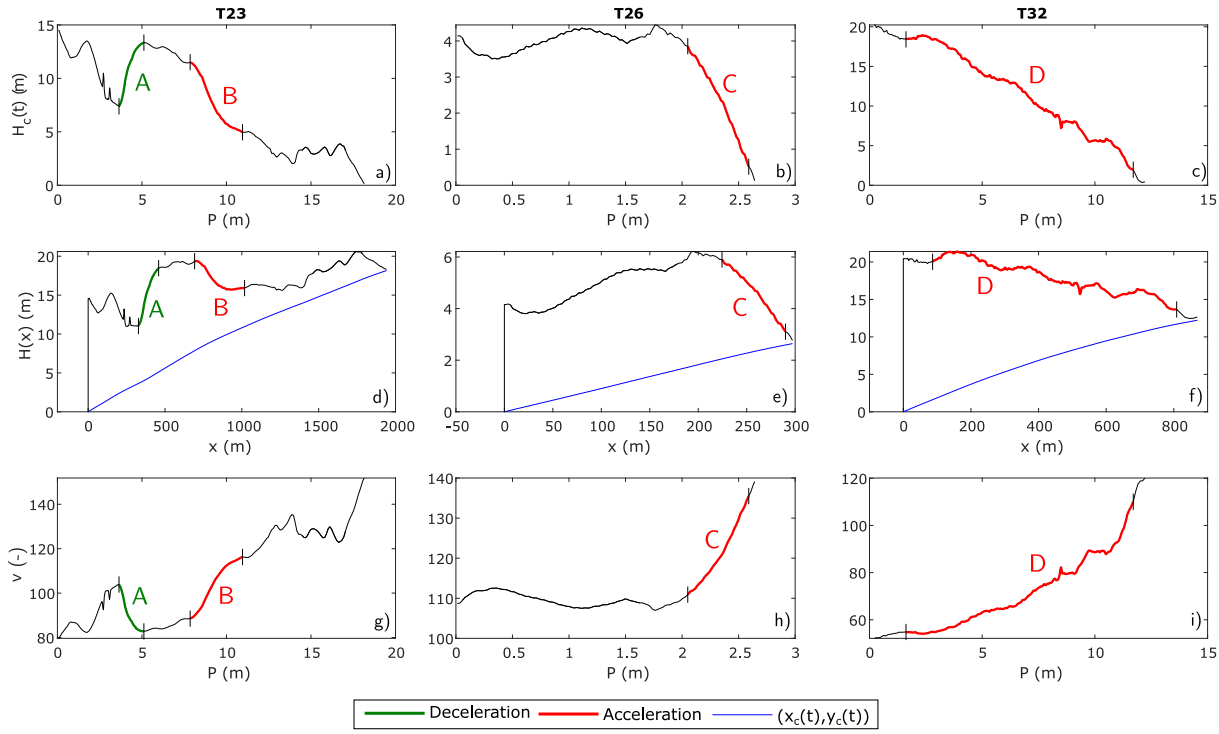

Figure 9. Panels (a–c) the cliff height of the 3 chosen transects as a function of P. Periods of notable deceleration (A) and acceleration (B) are highlighted with green and red respectively. The corresponding regions on the topography are also highlighted in panels (d–f), with the trajectory of the cliff toe (x_c, y_c) shown with a dashed blue line. Panels (g–i) v as a function of P indicating the changing magnitude of retreat over the life cycle of the cliffs. Figure created by the lead author. © University of Nottingham.

To highlight possible model behaviors, we identify intervals of monotonically decreasing (acceleration) and increasing (deceleration) H_c as P increases (see Figures 9a–9c). No period of consistent equilibrium behavior, that is where Equation 20 holds, is identified. For T23, intervals of strong deceleration (segment A) and acceleration (segment B) are identifiable, while for T26, only a monotonic acceleration (segment C) close to the time of typology change is seen. The cliff in T32 has a mostly negative inland slope causing acceleration (segment D) throughout the simulation period. The trajectory of the cliff toe (x_c, y_c) is plotted in Figures 9d, 9e and 9f). The effect of topography on this trajectory is best seen on T23, where changes of slope in segments A and B cause deceleration and acceleration respectively. The inverse of this slope is the non-dimensional retreat rate v, plotted in Figures 9g, 9h and 9i. The intervals of changing H_c correspond clearly to changes in v.

The correlation between $H_c(t = 0)$ and the threshold RSLR corresponding to typology change, is further explored in Figure 10. While $H_c(t = 0)$ could be intuitively considered an indicator of resilience of cliffs to RSLR, it does not take into account the effect of the inland topography. For this reason, the threshold can exceed $H_c(t = 0)$ (as in T10-12 and T22-24), or be less than $H_c(t = 0)$, as occurs in most transects tested along the Holderness coast, including T26 and T32 shown in previous figures.

6. Discussion

Figure 6a shows a clear discrepancy between modeled and observed historical retreat on the Holderness coast. It is not possible to directly isolate the contribution of RSLR on erosion rates from observations, but an order of magnitude estimate may be obtained. On the Holderness coast, we expect the modeled retreat to be lower than the observed retreat over the same period. This is due to the dominant longshore drift (Pye & Blott, 2015), which transports sediment southward toward Spurn Point and into the Humber Estuary. Additionally, the locations of eroded villages (Sheppard, 1912) suggest that the Holderness coast has been experiencing substantial erosion long before anthropogenic sea level rise. Therefore, we expect that sea level rise contributes a smaller proportion of cliff retreat here compared to other coastal regions. Between the years of 1852 and 2005, our model predicts a median proportion of 13.4% of observed retreat, in line with our expectations. Coastal defenses have existed in

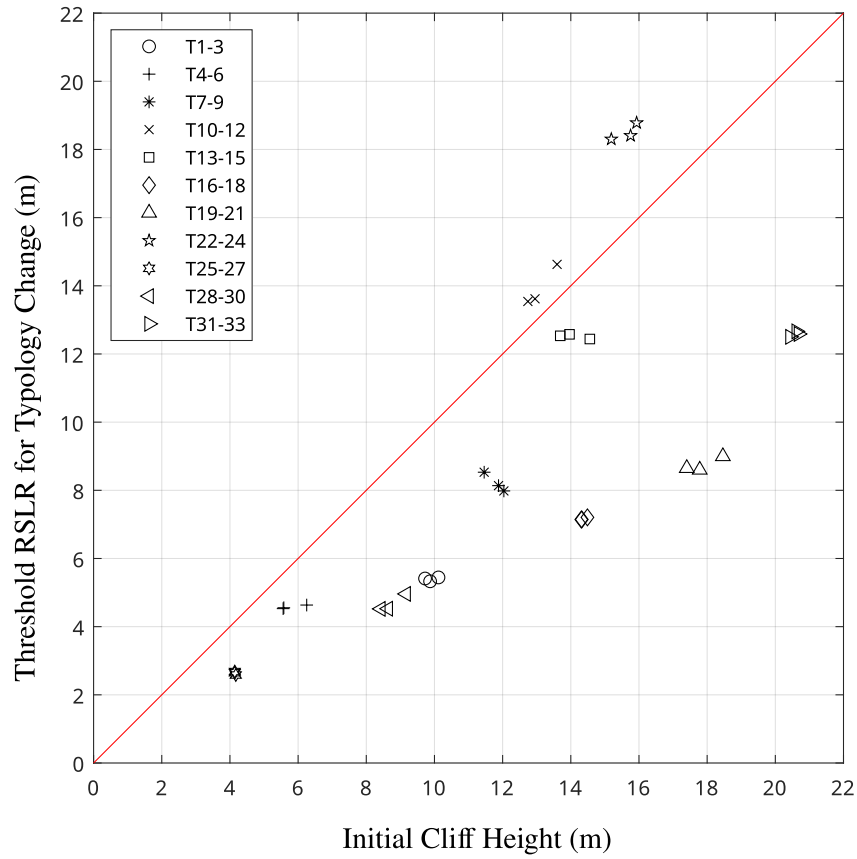

Figure 10. Initial cliff height plotted against threshold RSLR (an estimate considering the effect of a varying inland topography) for all 3 transects at all 11 locations. The correlation coefficient between the two indicators is 0.7107. Figure created by the lead author. © University of Nottingham.

some capacity at Hornsea and Withernsea for much of the observation period, and causes a gradient in retreat rates, clearly shown on Figure 6a. Our model will not reproduce the effects of coastal defenses, and this to some degree explains the longshore variation in the ratio of modeled and observed retreat seen in Figure 6b. Model predictions of future retreat show the importance of including the effect of inland topography in the simulation of multi-century evolution of soft cliff retreat. While many studies (Brooks & Spencer, 2012; Dickson et al., 2007; Limber et al., 2018) reach the conclusion that accelerating RSLR corresponds to accelerating cliff retreat, the present study illustrates that periods of decelerating recession can be a result of topographic variation (e.g., T23, see Figure 9). However, these correspond to brief sections of topography with steep positive slope, rather than being the dominant behavior at any studied location. Brooks and Spencer (2012) identify cliffs on the Suffolk coast where cliff heights may increase by 2095, however their modeling approach ignores the reduction in effective cliff height caused by RSLR, and is a shorter timescale study than this work.

Much focus of Wolinsky and Murray (2009) was on establishing equilibrium retreat rates. Using Equation 24, we calculate $P_{\frac{1}{2}} < 25$ for all transects, less than global sea level rise of 130 m since the end of the last ice age. Therefore, where a cliff can achieve equilibrium, it should be close to it. At this equilibrium, the non-dimensional rate of recession v is constant. However, we can see from Figures 9g–9i that v does not remain constant for long at the locations studied. This does not contradict our previous statement that cliffs which can achieve equilibrium due to having sufficiently steep and approximately constant inland slopes would be close to equilibrium, just that transects studied do not satisfy these conditions. For cliffed coasts with sufficient sediment availability to form an equilibrium beach profile, Ashton et al. (2011) proposes a "no-feedback" category of cliff retreat, where the coastal recession rate is proportional to the rate of RSLR. At equilibrium, this is true for our model, and our analysis of long-term behavior agrees with the scaling rules of Ashton et al. (2011).

The years when RSLR drives a transition from a soft cliffed coast to some other typology are indicated on Figure 8. According to our model, in a worst-case emissions scenario, these transitions start to occur in the next few hundred years. Even when forced with moderate GSLR projections, typology change across the Holderness coasts is likely to happen in the next two millennia. The processes governing coastal evolution during this transition are unknown. The times illustrated on Figure 8 are when the cliff toe meets the existing topography, however if the cliff top experiences regular flooding due to waves and storm surges, this transition may be considered to be already occurring. At T26 (Tunstall Beach), the most vulnerable location studied, fears of saltwater inundation with extreme sea level conditions have already led to some flood alleviation strategies to be put in place (Wood, 2021). These results suggest T26 is particularly close to typology transition, and this site is suitable for further investigation of this change.

One direction for future study would be to explore beyond typology change. If the coast were to transition to, for example, a dune-beach system (Rosati et al., 2013), a sandy coast with a barrier island (Murray & Moore, 2018), or a transgressing rocky profile (Walkden & Dickson, 2008), it would be interesting to understand the factors controlling the approach to each of these distinct geomorphological states. A full study of the drivers, controls and timescale of typology change, using more detailed process-based models, would develop the ideas initiated in this work. There are consistencies between the equilibrium behavior of this model and similar models for barrier island transgression (Murray & Moore, 2018). In particular, at equilibrium, the direction of every point on the profile matches the backshore slope. This may imply that piecewise application of existing equilibrium models may be good approximations of evolution beyond typology change. However, transitions in coastal type are far-from-equilibrium behaviors, contravening model assumptions, and this piecewise approach should be supported by more detailed modeling studies.

The importance of considering realistic topographies in regards to typology change is illustrated in Figure 10. Here, we compare a rudimentary measure of coastal resilience to sea level rise, the initial cliff height $H_c(t = 0)$ (since a taller cliff would be expected to experience a typology change later), to the RSLR required for transition according to our model. We see that broadly speaking, using $H_c(t = 0)$ as an indicator of vulnerability overestimates the resilience of these cliffs (as with T26 and T32). The downward sloping topographies of T19-21 and T31-33 means that they are more vulnerable to typology change than their tall cliffs present currently would suggest. Additionally, T13-15 and T31-33 have similar resilience, despite having quite different initial cliff heights. T10-12 and T22-24 are notable exceptions. In T23, this is due to periods of steeper slope and consequent deceleration, shown in Figure 9.

7. Limitations

We here discuss the effect of the assumptions of the present modeling on the results. In particular we focus on the representation of the depth of closure and both physical and geometric parameters used in the modeling.

7.1. Role of the Depth of Closure

In our model, adaptation to RSLR is expressed through accommodation. The accommodation process, as modeled in Wolinsky and Murray (2009), is heavily dependent on the depth of closure (Nicholls et al., 1998; Ortiz & Ashton, 2016), a theoretical limit to the influence of surface oceanic processes on seabed sediment transport. In this work, we choose the timescale dependent formula of Birkemeier (1985), however we tested four formulae (Birkemeier, 1985; Hallermeier, 1980, 1983; Houston, 1995) for the depth of closure, which give very different values (9.77, 12.95, 8.89 and 19.35 m, respectively) and there is no consensus on which formulation is most suitable for calculating the sediment demands of foreshore adaptation to RSLR (Cooper & Pilkey, 2004). We extended the formula of Birkemeier (1985) to a thousand-year timescale. The statistical extrapolation of the depth of closure concept to this timescale is not particularly robust, and is used in the absence of other methods. In this work, as in the classical Bruun rule (Bruun, 1962), we connect closure depth to accommodation space: the small probability of sediment being disturbed at the closure depth defines an area of seabed where material eroded from the cliff must collect. As sea level rises with no change in wave climate, the closure contour shifts landwards, as does the accommodation space. There is an argument to be made that if sea level rise is sufficiently rapid, then there is not enough time for the lower shoreface to respond, and form an equilibrium profile (Ortiz & Ashton, 2016). Further study should explore the relationship between the rate of profile adjustment, the curvature of the profile, and the rate of sea level rise, to determine a rate of RSLR where the equilibrium profile assumption

breaks down. We believe that having a similar closure timescale to modeling timescale is justified with this modeling approach. However, there are a number of definitions of closure depth for different applications, and a shorter morphodynamic timescale of a few decades—reflecting a timescale of shoreface response to sea level changes—may also be a valid approach. This model for accommodation is simplistic and further understanding of the sediment demands of foreshore adaptation to RSLR is key to improving reliability of this model.

The shore platform underlying the foreshore is assumed to have little influence on the response of the beach profile to RSLR. However, this assumption may be invalid if the shore platform has an influence on retreat (Payo et al., 2015), or the shape of a beach equilibrium profile (Trenhaile, 2004). The shore platform is difficult to detect on the Holderness Coast (Morgan et al., 2022) and other paraglacial coasts, due to its infrequent exposure, and most studies on equilibrium profile emergence focus on either sandy beach (Dean, 1991; Pilkey et al., 1993) or shore platform dominated coasts (Trenhaile, 2020; Walkden & Hall, 2005), rather than the combination of both needed for this study site.

7.2. Uncertainty of Parameters

Estimates of a number of parameters are needed to run the model. There is considerable uncertainty in projections of local RSLR over millennial timescales. We use global estimates of sea level rise, and use GIA as an additional driver of RSLR on the Holderness coast, which we believe is the most suitable approach given the study site and availability of projections of sea level rise over this timescale.

$VLM(t)$ is constant, since GIA is assumed constant. The review of Stockamp et al. (2015) used as a guideline for the chosen value of 0.5 mm/year. In reality GIA is time-varying, and is likely to slow as the ground level rebounds over the next 10,000 years (Shennan, 1989). Since the majority of our transects experience typology change in the next 2,000 years, this is unlikely to have a large influence on predictions, but over longer timescales a more detailed model of $VLM(t)$ may be needed. This also ignores other processes governing ground movement (Shennan, 1989), for example additional tectonic processes and natural sediment compaction, and possible local variation in uplift and subsidence. The initial MLWL is estimated from modeled spring and neap tides for two locations tens of kilometers away from the Holderness coast (National Tidal and Sea Level Facility, 2024). Accurately determining H_t is made difficult by the presence of taluses on many transects. In this study, the cliff profile is approximated by a right-angled triangle, and the center of mass of this triangle taken as the shoreline position. Over the modeling timescale, predictions are not overly sensitive to this approximation. However, an improved parametrization of cliff shape, taking into account geotechnical factors, even as cliff height changes, would be a logical inclusion where available.

In the validation against historical retreat, we assume current cliff composition, wave climate and eroded topography are similar to the historical environment. For the intended order-of-magnitude estimate, this is justified, especially since high-resolution data is not available over the timescale modeled. More detailed estimates of historical topography would improve the reliability of the model.

Geology is here simplified; where geological inhomogeneity is notable (Valvo et al., 2006), a time and spatially varying value of $\bar{c}$ may be necessary. The values of ϕ_b, ϕ_c and s_f are found through secondary sources, but a local granulometry study (Allen & Haslett, 2006) would lead to more reliable estimates.

This study generalizes the work of Wolinsky and Murray (2009) by introducing a time-varying cliff height and rate of sea level rise. Variation in $VLM(t)$ and $\bar{c}$ may be introduced naturally into the modeling framework, in locations where this variation is considered influential on retreat, and where sufficient data sets are available. Time variation in other parameters, especially closure depth, could be introduced if additional evidence (e.g., further modeling studies or morphological measurements) suggests fundamental modeling assumptions hold, even as these parameters change.

The relative importance of each parameter for predicting both erosion rates and the timing of typology change should be explored through a global sensitivity analysis (Iooss & Lemaître, 2015; Saltelli et al., 2008). Model reliability could then be efficiently improved by focusing efforts on reducing the uncertainty in the most important parameters.

8. Conclusions

This work aims to develop a model suitable for simulation of soft cliffed coast evolution in response to time-dependent sea level rise scenarios over multi-century timescales. The model is intended to provide an indication of the natural (unmanaged) evolution of this coastal type, and accounts for complex inland topographies. The model equation can be solved analytically for simple linear topographies and any strictly increasing relative sea level rise scenario. An analysis of long-term model behavior shows that an equilibrium retreat rate is only possible when the inland topography is sufficiently steep and smooth. Within the model, a change in coastal typology, corresponding to the disappearance of the cliff, may occur. Capabilities of the model are explored through application to the Holderness coast in East Yorkshire, UK. We first validate the model by comparison to observed retreat on the Holderness coast over a 153 years time period. The model predicts a median of 13.4% of historical erosion is driven by sea level rise, this is expected for this coast. We then force current coastal profiles with a set of future sea level rise scenarios. This application predicts that over the modeled timescale, accelerating relative sea level rise results in accelerating cliff retreat at all locations, in line with previous research (Brooks & Spencer, 2012; Dickson et al., 2007; Limber et al., 2018). However, topographic variation can lead to more complex behaviors including temporary deceleration of cliff recession (see Figure 9). We demonstrate that the inland topography is also an important factor in determining the timing of typology change. We therefore propose the use of critical relative sea level rise corresponding to typology change, which incorporates the effect of topography, as an indicator of cliff resilience to sea level rise, instead of current cliff height.

The processes governing a coast during and after cliff disappearance are not explored in this work. A further understanding of these transitions, through identifying and observing vulnerable areas and modeling studies, would give insight into the life-cycle of coastal environments. A key limitation of this study, the uncertainty in choice of the depth of closure, highlights the need for further research to determine which formula is most appropriate for use in coastal evolution models that cover multi-century timescales. Furthermore, using the current assumptions and available modeling approaches, a natural next step for this study is a global sensitivity analysis to determine the most important factors impacting future erosion rate and timing of typology change.

Appendix A: Model Solution for $u(t)$

We write Equation 7 in a more compact form:

$$u' = \frac{R'u}{R} - \frac{u^2}{\bar{c}L_s} - \frac{S_0 u^3}{\bar{c}L_s R}, \tag{A1}$$

noting that $u, u' = \frac{du}{dt}, R, R' = \frac{dR}{dt}$ are functions of time t, and the other quantities are constant. Then we use the substitution $v(t) = \frac{u}{R}$,

$$Rv' + R'v = R'v - \frac{R^2v^2}{\bar{c}L_s} - \frac{S_0R^2v^3}{\bar{c}L_s}. \tag{A2}$$

v is therefore the non-dimensional retreat rate as a function of time. We can then rearrange so

$$v' = -\frac{R}{\bar{c}L_s}\left(v^2 + S_0v^3\right). \tag{A3}$$

The case where $S_0 = 0$ is trivial in comparison to the non-zero case, and hereafter will only be included in the full analytic solutions. Since S_0 is a constant, this equation is separable:

$$\int \frac{1}{v^2(1+S_0v)}dv = -\frac{1}{\bar{c}L_s}\int R(t)dt. \tag{A4}$$

We can solve the left hand side of the equation using partial fractions. Also, let $P(t) = \int_0^t R(\rho)d\rho$ (introducing ρ as a dummy variable), equal to the cumulative change in RSLR between the initial time and time t. Integration of both sides leads to the equation

$$-S_0 \ln|v| - \frac{1}{v} + S_0 \ln|1 + S_0 v| = -\frac{P(t)}{\bar{c} L_s} + a_0, \tag{A5}$$

where a_0 is constant. We can combine the logarithms, and divide through by S_0 to get

$$\ln|S_0\left(1 + \frac{1}{S_0 v}\right)| - \frac{1}{S_0 v} = -\frac{P(t)}{\bar{c} L_s S_0} + \frac{a_0}{S_0}. \tag{A6}$$

By letting $w = -1 - \frac{1}{S_0 v}$, the expression becomes:

$$\ln|-S_0 w| + w = -\frac{P(t)}{\bar{c} L_s S_0} + \frac{a_0}{S_0} - 1. \tag{A7}$$

Exponentiating both sides gives

$$|-S_0 w| \exp(w) = \exp\left(\frac{a_0}{S_0} - 1\right) \exp\left[-\frac{P(t)}{\bar{c} L_s S_0}\right], \tag{A8}$$

whatever the signs of S_0 and w, both sides can be divided by either positive or negative S_0, which can be incorporated into the integrating constant

$$w \exp(w) = a_1 \exp\left[-\frac{P(t)}{\bar{c} L_s S_0}\right], \tag{A9}$$

where $a_1 = -\text{sgn}(S_0)\,\text{sgn}(w)\exp\left(\frac{a_0}{S_0} - 1\right)$. We can use the Lambert W function (Corless et al., 1996) to get a closed form expression for w:

$$w = W\left(a_1 \exp\left[-\frac{P(t)}{\bar{c} L_s S_0}\right]\right). \tag{A10}$$

Then, by combining Equation A10 with the definitions of w and v we get an expression for u, Equation A11.

$$u(t) = \begin{cases} -\dfrac{R(t)}{S_0\left[W_0\left(a_1 \exp\left[-\dfrac{P(t)}{\bar{c} L_s S_0}\right]\right) + 1\right]} & S_0 > 0 \\ -\dfrac{\bar{c} L_s R(t)}{H_s + H_c(t=0) - P(t)} & S_0 = 0 \\ -\dfrac{R(t)}{S_0\left[W_{-1}\left(a_1 \exp\left[-\dfrac{P(t)}{\bar{c} L_s S_0}\right]\right) + 1\right]} & S_0 < 0. \end{cases} \tag{A11}$$

Appendix B: Branches of the Lambert W Function

The branch used to calculate cliff retreat depends on the profile geometry, and controls the long-term behavior of the system. If $S_0 > 0$, the branch of the Lambert W function used is W_0 and if $S_0 < 0$, W_{-1} is used. This is proven as follows. The boundary between $W_0(x)$ and $W_{-1}(x)$ is where $W(x) = -1$. When $W\left(a_1 \exp\left[-\frac{P(t)}{\bar{c} L_s S_0}\right]\right) = -1$, $H_c(t) = -H_s$ which is impossible. Therefore the branch used cannot change as the system evolves, and the branch chosen depends only on the initial state of the system, which is expressed through the constant a_1. The principal branch is therefore used if $W(a_1) > -1$, or equivalently, $\frac{H_c(t=0)+H_s}{\bar{c} L_s S_0} > 0$. This occurs if and only if $S_0 > 0$. The logic for the secondary branch is similar, proving our initial statement.

Appendix C: Model Solution for $x_c(t)$

Integrating both sides of Equation A11, and using the definition $u = \frac{dx_c}{dt}$:

$$x_c(t) = -\frac{1}{S_0}\int \frac{1}{W\left(a_1 \exp\left[-\frac{P(t)}{\overline{c}L_s S_0}\right]\right) + 1}\frac{dP}{dt}dt. \tag{C1}$$

We use a substitution, letting $\eta = a_1 \exp\left(-\frac{P(t)}{\overline{c}L_s S_0}\right)$, so $\frac{d\eta}{dt} = -\frac{1}{\overline{c}L_s S_0}\eta\frac{dP}{dt}$ and find

$$x_c(P) = \overline{c}L_s \int \frac{1}{\eta[W(\eta)+1]}d\eta. \tag{C2}$$

Next, let $\xi = W(\eta)$. The derivative of the Lambert W function means that $\frac{d\xi}{d\eta} = \frac{\xi}{\eta(1+\xi)}$. This final change of variables leads to the equation,

$$x_c(P) = \overline{c}L_s \int \frac{1}{\xi}d\xi, \tag{C3}$$

leading to the solution,

$$x_c(P) = \overline{c}L_s \ln|\xi| + a_2. \tag{C4}$$

A final resubstitution yields the general analytical solution Equation 15, noting that $a_2 = -\overline{c}L_s \ln|W(a_1)|$, and logarithms can be combined. The absolute value function is dropped, since the signs of $W(a_1)$ and $W\left(a_1 \exp\left(-\frac{P}{\overline{c}L_s S_0}\right)\right)$ are equal, so the quantity inside the logarithm is always positive.

Conflict of Interest

The authors declare no conflicts of interest relevant to this study.

Data Availability Statement

The model scripts and data generated by this work are available for download on Zenodo (Appleton et al., 2024), available for use under a Creative Commons Attribution licence. The Surfzone DEM is available from https://www.data.gov.uk/dataset/fe455db0-5ce5-4d63-8b38-d74612eb43d5/surfzone-digital-elevation-model-dem-2m, under an Open Government Licence, allowing the publishing of data for non-commercial purposes, with copyright owned by the Environment Agency, East Riding of Yorkshire Coastal Monitoring Programme, and the Northeast Regional Coastal Monitoring Programme, shown on Figure 5. The LiDAR composite DEM is available from https://www.data.gov.uk/dataset/7f31af0f-bc98-4761-b4b4-147bfb986648/lidar-composite-digital-terrain-modeldtm-10m, under an Open Government Licence, allowing the publishing of data for non-commercial purposes, with copyright owned by the Environment Agency, shown on Figure 5. The OceanWise bathymetry data is available for purchase at https://digimap.edina.ac.uk/marine, for this study this was accessed using an institutional subscription. The End User License Agreement allows the publishing of small extracts of OceanWise Data in academic articles for Educational Purposes, shown on Figure 5. The Holderness retreat data is detailed in Brown et al. 2012, reproduced on Figure 6, and is available on request from the authors. The sea level rise scenarios used to force the model are available in the supplementary material of Clark et al. 2016, reproduced on Figure 3. The tidal data was obtained from https://ntslf.org/tides/uk-network/predictions-hilo, copyright owned by the National Oceanographic Centre (NOC), with permission to download and copy data for individual research. The ERA5 reanalysis data is available from https://cds.climate.copernicus.eu/datasets/reanalysis-era5-single-levels?tab=overview, available for use under a CC-BY licence, with copyright owned by Copernicus Climate Change Service (C3S).

Acknowledgments
This work was supported by the Natural Environment Research Council (NERC), U.K., with M.A.'s studentship through the Envision Doctoral Training Partnership (NE/S007423/1). A.P. was funded by the CHAMFER project (NE/W004992/1). We would like to thank Sally Brown for access to Holderness coast historical retreat data and Asunción Baquerizo for manuscript feedback. This work was published with the permission of the Director of the British Geological Survey (UKRI). We acknowledge BGS support for the PhD via the BUFI (British Geological Survey University Funding Initiative) mechanism.

References

Allen, J. R. L., & Haslett, S. K. (2006). Granulometric characterization and evaluation of annually banded mid-Holocene estuarine silts, Welsh Severn Estuary (UK): Coastal change, sea level and climate. *Quaternary Science Reviews*, *25*(13–14), 1418–1446. https://doi.org/10.1016/j.quascirev.2005.12.009

Appleton, M., Briganti, R., Dodd, N., & Payo, A. (2024). A mass conservation model to study the evolution of coastal soft cliffs driven by sea level rise over multi-century timescales [Dataset]. *Zenodo*. https://doi.org/10.5281/zenodo.13829366

Ashton, A. D., Walkden, M. J. A., & Dickson, M. E. (2011). Equilibrium responses of cliffed coasts to changes in the rate of sea level rise. *Marine Geology*, *284*(1–4), 217–229. https://doi.org/10.1016/j.margeo.2011.01.007

Barnard, P. L., Dugan, J. E., Page, H. M., Wood, N. J., Hart, J. A. F., Cayan, D. R., et al. (2021). Multiple climate change-driven tipping points for coastal systems. *Scientific Reports*, *11*(1), 15560. https://doi.org/10.1038/s41598-021-94942-7

Bell, F. G. (2002). The geotechnical properties of some till deposits occurring along the coastal areas of Eastern England. *Engineering Geology*, *63*(1–2), 49–68. https://doi.org/10.1016/s0013-7952(01)00068-0

Bell, F. G., & Forster, A. (1991). The geotechnical characteristics of the till deposits of Holderness. *Geological Society, London, Engineering Geology Special Publications*, *7*(1), 111–118. https://doi.org/10.1144/gsl.eng.1991.007.01.07

Beuzen, T., Turner, I. L., Blenkinsopp, C. E., Atkinson, A., Flocard, F., & Baldock, T. E. (2018). Physical model study of beach profile evolution by sea level rise in the presence of seawalls. *Coastal Engineering*, *136*, 172–182. https://doi.org/10.1016/j.coastaleng.2017.12.002

Birkemeier, W. A. (1985). Field data on seaward limit of profile change. *Journal of Waterway, Port, Coastal, and Ocean Engineering*, *111*(3), 598–602. https://doi.org/10.1061/(asce)0733-950x(1985)111:3(598)

Bodge, K. R. (1992). Representing equilibrium beach profiles with an exponential expression. *Journal of Coastal Research*, 47–55.

Bosboom, J., & Stive, M. J. F. (2021). *Coastal dynamics*. TU Delft Open.

Bray, M. J., & Hooke, J. M. (1997). Prediction of soft-cliff retreat with accelerating sea-level rise. *Journal of Coastal Research*, 453–467.

Bricheno, L., Amies, J. D., Chowdhury, P., Woolf, D. K., & Timmermans, B. (2023). *Climate change impacts on storms and waves relevant to the UK and Ireland*. MCCIP Science Review.

Brooks, S. M., & Spencer, T. (2012). Shoreline retreat and sediment release in response to accelerating sea level rise: Measuring and modelling cliffline dynamics on the Suffolk Coast, UK. *Global and Planetary Change*, *80*, 165–179. https://doi.org/10.1016/j.gloplacha.2011.10.008

Brown, S., Barton, M. E., & Nicholls, R. J. (2012). The effect of coastal defences on cliff top retreat along the Holderness coastline. *Proceedings of the Yorkshire Geological Society*, *59*(1), 1–13. https://doi.org/10.1144/pygs.59.1.288

Bruun, P. (1962). Sea-level rise as a cause of shore erosion. *Journal of the Waterways and Harbors Division*, *88*(1), 117–130. https://doi.org/10.1061/jwheau.0000252

Castedo, R., Murphy, W., Lawrence, J., & Paredes, C. (2012). A new process-response coastal recession model of soft rock cliffs. *Geomorphology*, *177*, 128–143. https://doi.org/10.1016/j.geomorph.2012.07.020

Clark, P. U., Shakun, J. D., Marcott, S. A., Mix, A. C., Eby, M., Kulp, S., et al. (2016). Consequences of twenty-first-century policy for multi-millennial climate and sea-level change. *Nature Climate Change*, *6*(4), 360–369. https://doi.org/10.1038/nclimate2923

Cooper, J. A. G., & Pilkey, O. H. (2004). Sea-level rise and shoreline retreat: Time to abandon the Bruun rule. *Global and Planetary Change*, *43*(3–4), 157–171. https://doi.org/10.1016/j.gloplacha.2004.07.001

Corless, R. M., Gonnet, G. H., Hare, D. E. G., Jeffrey, D. J., & Knuth, D. E. (1996). On the Lambert W function. *Advances in Computational Mathematics*, *5*, 329–359.

D'Anna, M., Idier, D., Castelle, B., Vitousek, S., & Le Cozannet, G. (2021). Reinterpreting the Bruun rule in the context of equilibrium shoreline models. *Journal of Marine Science and Engineering*, *9*(9), 974.

Dean, R. G. (1991). Equilibrium beach profiles: Characteristics and applications. *Journal of Coastal Research*, 53–84.

De Leo, F., Briganti, R., & Besio, G. (2023). Trends in ocean waves climate within the Mediterranean Sea: A review. *Climate Dynamics*, *62*(2), 1–12. https://doi.org/10.1007/s00382-023-06984-4

Dickson, M. E., Walkden, M. J. A., & Hall, J. W. (2007). Systemic impacts of climate change on an eroding coastal region over the twenty-first century. *Climatic Change*, *84*(2), 141–166. https://doi.org/10.1007/s10584-006-9200-9

Dornbusch, U., & Mylroie, P. (2018). Examples of coastal catch-up including barrier roll-back, marsh and brick-Earth cliff erosion in Southeast England. In *Coasts, marine structures and breakwaters 2017: Realising the potential* (pp. 83–92). ICE Publishing.

Environment Agency, U.K. (2019). SurfZone digital elevation model 2019 [Dataset]. Retrieved from https://www.data.gov.uk/dataset/fe455db0-5ce5-4d63-8b38-d74612eb43d5/surfzone-digital-elevation-model-2019

Environment Agency, U.K. (2022). LIDAR composite DTM 2022 – 10m [Dataset]. Retrieved from https://www.data.gov.uk/dataset/7f31af0f-bc98-4761-b4b4-147bfb986648/lidar-composite-dtm-2022-10m

Fox-Kemper, B., Hewitt, H., Xiao, C., Drijfhout, S. S., Edwards, T. L., Aðalgeirsdóttir, G., et al. (2021). Ocean, cryosphere and sea level change [Book Section]. In V. Masson-Delmotte, et al., (Eds.), *Climate change 2021: The physical science basis. Contribution of working group I to the sixth assessment report of the intergovernmental panel on climate change (chap. 9)*. Cambridge University Press. Retrieved from https://www.ipcc.ch/report/ar6/wg1/downloads/report/IPCC_AR6_WGI_Chapter09.pdf

Glavovic, B., Dawson, R., Chow, W., Garschagen, M., Haasnoot, M., Singh, C., & Thomas, A. (2022). Cities and settlements by the sea [Book Section]. In H. O. Pörtner, et al. (Eds.), *Climate change 2022: Impacts, adaptation and vulnerability. Contribution of working group II to the sixth assessment report of the intergovernmental panel on climate change*. Cambridge University Press.

Groll, N., Grabemann, I., & Gaslikova, L. (2014). North sea wave conditions: An analysis of four transient future climate realizations. *Ocean Dynamics*, *64*, 1–12. https://doi.org/10.1007/s10236-013-0666-5

Hallermeier, R. J. (1980). A profile zonation for seasonal sand beaches from wave climate. *Coastal Engineering*, *4*, 253–277. https://doi.org/10.1016/0378-3839(80)90022-8

Hallermeier, R. J. (1983). Sand transport limits in coastal structure designs. In *Coastal structures* (pp. 703–716).

Hersbach, H., Bell, B., Berrisford, P., Biavati, G., Horányi, A., Muñoz Sabater, J. J., Thépaut, J.-N., et al. (2023). ERA5 hourly data on single levels from 1940 to present. [Dataset]. *Copernicus Climate Change Service (C3S) Climate Data Store (CDS)*. https://doi.org/10.24381/cds.adbb2d47

Highest and lowest predicted tides / National Tidal and Sea Level Facility. (2024). Highest and lowest predicted tides/national tidal and sea level facility [Dataset]. Retrieved from https://ntslf.org/tides/hilo

Hobbs, P., Jones, L., Kirkham, M., Morgan, D., Pennington, C., Jenkins, G., et al. (2013). *Slope dynamics project report. Holderness Coast—Aldbrough, survey and monitoring, 2001–2013*. (Tech. Rep.). British Geological Survey.

Hobbs, P., Pennington, C., Pearson, S., Jones, L., Foster, C., Lee, J., & Gibson, A. (2008). *Slope dynamics project report. Norfolk Coast (2000–2006)*. (Tech. Rep.). British Geological Survey.

Holthuijsen, L. (2010). *Waves in oceanic and coastal waters*. Cambridge University Press.
Houston, J. R. (1995). Beach-fill volume required to produce specified dry beach width. *Coastal Engineering Technical Note*, 11–32.
Hudson, T., Keating, K., & Pettit, A. (2015). *Cost estimation for coastal protection – Summary of evidence*. (Tech. Rep.). Environment Agency.
Iooss, B., & Lemaître, P. (2015). A review on global sensitivity analysis methods. In *Uncertainty management in simulation-optimization of complex systems: Algorithms and applications* (pp. 101–122).
Ivins, E. R., & Wolf, D. (2008). Glacial isostatic adjustment: New developments from advanced observing systems and modeling. *Journal of Geodynamics*, *46*(3–5), 69–77. https://doi.org/10.1016/j.jog.2008.06.002
Jevrejeva, S., Moore, J. C., Grinsted, A., Matthews, A. P., & Spada, G. (2014). Trends and acceleration in global and regional sea levels since 1807. *Global and Planetary Change*, *113*, 11–22. https://doi.org/10.1016/j.gloplacha.2013.12.004
Klinck, B. A., Hopson, P. N., Morigi, A. N., Bloodworth, A. J., Inglethorpe, S. D. J., Entwisle, D. C., & Wealthall, G. P. (1997). *The hydrogeological classification of superficial clay: The hydrogeological characterisation of glacial till in East Anglia*. (Tech. Rep.). Environment Agency.
Lambeck, K., Rouby, H., Purcell, A., Sun, Y., & Sambridge, M. (2014). Sea level and global ice volumes from the last glacial maximum to the Holocene. *Proceedings of the National Academy of Sciences*, *111*(43), 15296–15303. https://doi.org/10.1073/pnas.1411762111
Le Cozannet, G., Garcin, M., Yates, M., Idier, D., & Meyssignac, B. (2014). Approaches to evaluate the recent impacts of sea-level rise on shoreline changes. *Earth-Science Reviews*, *138*, 47–60. https://doi.org/10.1016/j.earscirev.2014.08.005
Lee, M. (2002). *Soft cliffs. Prediction of recession rates and erosion control techniques*. (Tech. Rep.). Department for Environment, Food and Rural Affairs.
Lee, M. (2018). *Coastal catch-up: How a soft rock cliff evolves when coastal defences fail*. (Tech. Rep.). Natural England Commissioned Reports.
Limber, P. W., Barnard, P. L., Vitousek, S., & Erikson, L. H. (2018). A model ensemble for projecting multidecadal coastal cliff retreat during the 21st century. *Journal of Geophysical Research: Earth Surface*, *123*(7), 1566–1589. https://doi.org/10.1029/2017jf004401
Lopez De San Roman Blanco, B., Woods Ballard, B., Simm, J., Brampton, A., Sutherland, J., Gouldby, B., & Rossington, K. (2019). *Coastal morphological modelling for decision-makers*. (Tech. Rep.). Environment Agency.
Morgan, D., Gunn, D., Payo, A., & Raines, M. (2022). Passive seismic surveys for beach thickness evaluation at different England (UK) sites. *Journal of Marine Science and Engineering*, *10*(5), 667. https://doi.org/10.3390/jmse10050667
Murray, A. B., Coco, G., Ashton, A. D., Moore, L., McNamara, D., & Limber, P. (2021). *Modeling nearshore, barrier, cliff, and coastline morphodynamics*. Elsevier.
Murray, A. B., & Moore, L. (2018). Geometric constraints on long-term barrier migration: From simple to surprising. In *Barrier dynamics and response to changing climate* (pp. 211–241). Springer International Publishing. https://doi.org/10.1007/978-3-319-68086-6_7
Nicholls, R. J., Birkemeier, W. A., & Lee, G.-h. (1998). Evaluation of depth of closure using data from Duck, NC, USA. *Marine Geology*, *148*(3–4), 179–201. https://doi.org/10.1016/s0025-3227(98)00011-5
OceanWise. (2020). Marine DEM 1 arc second [Dataset]. Retrieved from https://digimap.edina.ac.uk/marine
Oppenheimer, M., Glavovic, B., Hinkel, J., van de Wal, R. S. W., Magnan, A. K., Cai, R., et al. (2020). *Sea level rise and implications for low lying Islands, coasts and communities*. The Ocean and Cryosphere in a Changing Climate. https://www.cambridge.org/core/books/ocean-and-cryosphere-in-a-changing-climate/sea-level-rise-and-implications-for-lowlying-islands-coasts-and-communities/5D756335C9C3A6DDFAE0219073349E8D
Ortiz, A. C., & Ashton, A. D. (2016). Exploring shoreface dynamics and a mechanistic explanation for a morphodynamic depth of closure. *Journal of Geophysical Research: Earth Surface*, *121*(2), 442–464. https://doi.org/10.1002/2015jf003699
Passeri, D. L., Hagen, S. C., Medeiros, S. C., Bilskie, M. V., Alizad, K., & Wang, D. (2015). The dynamic effects of sea level rise on low-gradient coastal landscapes: A review. *Earth's Future*, *3*(6), 159–181. https://doi.org/10.1002/2015ef000298
Payo, A., Favis-Mortlock, D., Dickson, M. E., Hall, J. W., Hurst, M., Walkden, M. J. A., et al. (2016). Coastalme version 1.0: A coastal modelling environment for simulating decadal to centennial morphological changes. *Geoscientific Model Development Discussions*, *2016*, 1–45.
Payo, A., Hall, J. W., Dickson, M. E., & Walkden, M. J. A. (2015). Feedback structure of cliff and shore platform morphodynamics. *Journal of Coastal Conservation*, *19*(6), 847–859. https://doi.org/10.1007/s11852-014-0342-z
Payo, A., & Walkden, M. J. A. (2018). Modelling rapid coastal catch-up after defence removal along the soft cliff coast of Happisburgh, UK. *Coastal Engineering Proceedings*, *1*(36), 63. https://doi.org/10.9753/icce.v36.sediment.63
Payo, A., Williams, C., Vernon, R., Hulbert, A. G., Lee, K. A., & Lee, J. R. (2020). Geometrical analysis of the inland topography to assess the likely response of wave-dominated coastline to sea level: Application to Great Britain. *Journal of Marine Science and Engineering*, *8*(11), 866. https://doi.org/10.3390/jmse8110866
Pilkey, O. H., Young, R. S., Rîggs, S. R., Smith, A. S., Wu, H., & Pilkey, W. D. (1993). The concept of shoreface profile of equilibrium: A critical review. *Journal of Coastal Research*, 255–278.
Pringle, A. W. (1985). Holderness coast erosion and the significance of ords. *Earth Surface Processes and Landforms*, *10*(2), 107–124. https://doi.org/10.1002/esp.3290100204
Pye, K., & Blott, S. (2015). Spatial and temporal variations in soft-cliff erosion along the Holderness coast, East riding of Yorkshire, UK. *Journal of Coastal Conservation*, *19*(6), 785–808. https://doi.org/10.1007/s11852-015-0378-8
Ranasinghe, R. (2020). On the need for a new generation of coastal change models for the 21st century. *Scientific Reports*, *10*(1), 2010. https://doi.org/10.1038/s41598-020-58376-x
Reguero, B. G., Losada, I. J., & Méndez, F. J. (2019). A recent increase in global wave power as a consequence of oceanic warming. *Nature Communications*, *10*(1), 205. https://doi.org/10.1038/s41467-018-08066-0
Riedel, H. P., & Byrne, A. P. (1987). Random breaking waves–horizontal seabed. In *Coastal engineering* (pp. 903–908).
Román-Sierra, J., Muñoz-Perez, J. J., & Navarro-Pons, M. (2014). Beach nourishment effects on sand porosity variability. *Coastal Engineering*, *83*, 221–232.
Rosati, J. D., Dean, R. G., & Walton, T. L. (2013). The modified Bruun rule extended for landward transport. *Marine Geology*, *340*, 71–81. https://doi.org/10.1016/j.margeo.2013.04.018
Saltelli, A., Ratto, M., Andres, T., Campolongo, F., Cariboni, J., Gatelli, D., et al. (2008). *Global sensitivity analysis: The primer*. John Wiley & Sons.
Shand, T., Shand, R., Reinen-Hamill, R., Carley, J., & Cox, R. (2013). A review of shoreline response models to changes in sea level. In *Coasts and ports* (Vol. 2013, p. 21).
Shennan, I. (1989). Holocene crustal movements and sea-level changes in Great Britain. *Journal of Quaternary Science*, *4*(1), 77–89. https://doi.org/10.1002/jqs.3390040109
Sheppard, T. (1912). *The lost towns of the Yorkshire coast*. A. Brown & Sons, Limited.

Stockamp, J., Bishop, P., Li, Z., Petrie, E. J., Hansom, J., & Rennie, A. (2015). State-of-the-art in studies of glacial isostatic adjustment for the British Isles: A literature review. *Earth and Environmental Science Transactions of the Royal Society of Edinburgh*, *106*(3), 145–170. https://doi.org/10.1017/s1755691016000074

Swift, D. J. P., & Thorne, J. A. (1992). Sedimentation on continental margins, I: A general model for shelf sedimentation. In *Shelf sand and sandstone bodies: Geometry, facies and sequence stratigraphy* (pp. 1–31).

Teixeira, R., Nogal, M., & O'Connor, A. (2018). On the suitability of the generalized Pareto to model extreme waves. *Journal of Hydraulic Research*, *56*(6), 755–770. https://doi.org/10.1080/00221686.2017.1402829

Trenhaile, A. (2004). Modeling the accumulation and dynamics of beaches on shore platforms. *Marine Geology*, *206*(1–4), 55–72. https://doi.org/10.1016/j.margeo.2004.03.013

Trenhaile, A. (2020). Modelling the development of dynamic equilibrium on shore platforms. *Marine Geology*, *427*, 106227. https://doi.org/10.1016/j.margeo.2020.106227

Valvo, L. M., Murray, A. B., & Ashton, A. D. (2006). How does underlying geology affect coastline change? An initial modeling investigation. *Journal of Geophysical Research*, *111*(F2). https://doi.org/10.1029/2005jf000340

Van Breedam, J., Goelzer, H., & Huybrechts, P. (2020). Semi-equilibrated global sea-level change projections for the next 10,000 years. *Earth System Dynamics Discussions*, *2020*(4), 1–35. https://doi.org/10.5194/esd-11-953-2020

Visvalingam, M., & Whyatt, J. D. (1990). The Douglas-Peucker algorithm for line simplification: Re-evaluation through visualization. *Computer Graphics Forum*, *9*(3), 213–225. https://doi.org/10.1111/j.1467-8659.1990.tb00398.x

Walkden, M. J. A., & Dickson, M. E. (2008). Equilibrium erosion of soft rock shores with a shallow or absent beach under increased sea level rise. *Marine Geology*, *251*(1–2), 75–84. https://doi.org/10.1016/j.margeo.2008.02.003

Walkden, M. J. A., & Hall, J. W. (2005). A predictive mesoscale model of the erosion and profile development of soft rock shores. *Coastal Engineering*, *52*(6), 535–563. https://doi.org/10.1016/j.coastaleng.2005.02.005

Walkden, M. J. A., & Hall, J. W. (2011). A mesoscale predictive model of the evolution and management of a soft-rock coast. *Journal of Coastal Research*, *27*(3), 529–543. https://doi.org/10.2112/jcoastres-d-10-00099.1

Whitehouse, P. L. (2018). Glacial isostatic adjustment modelling: Historical perspectives, recent advances, and future directions. *Earth Surface Dynamics*, *6*(2), 401–429. https://doi.org/10.5194/esurf-6-401-2018

Wolinsky, M. A. (2009). A unifying framework for shoreline migration: 1. Multiscale shoreline evolution on sedimentary coasts. *Journal of Geophysical Research*, *114*(F1). https://doi.org/10.1029/2007jf000855

Wolinsky, M. A., & Murray, A. B. (2009). A unifying framework for shoreline migration: 2. Application to wave-dominated coasts. *Journal of Geophysical Research*, *114*(F1). https://doi.org/10.1029/2007jf000856

Wood, A. (2021). £600,000 flood protection scheme "should stop tidal surge cutting off southern Holderness" [Newspaper Article]. *Yorkshire Post*. Retrieved from https://www.yorkshirepost.co.uk/news/people/ps600000-flood-protection-scheme-should-stop-tidal-surge-cutting-off-southern-holderness-3175909